CRYSTAL SPECTROSCOPY AT THE JOHNS HOPKINS UNIVERSITY *

H. M. Crosswhite and H. W. Moos **

The Johns Hopkins University, Baltimore, Maryland

ABSTRACT

Comparison of the free ion and crystal energy $4f^N$ levels is given for SmIII, HoIII, PrIV and ErIV. For the divalent spectra a general depression of some 12,000 cm^{-1} for the 5d crystal bands relative to the free ion levels can also be seen. The relationships for the trivalent ions are not yet very clear.

Spectrum lines of Ho^{3+} in $LaCl_3$ show a wide range of sharpness; for some, which require resolving powers in excess of 600,000, detailed hyperfine structure studies are being made.

The trichloride lattice vibronic sidebands associated with Pr^{3+} and Nd^{3+} in $NdCl_3$ have been studied in absorption. They show that 1) vibronics of the same type are identical in frequency for the two ions, 2) the number of vibronics is very much greater than the number of vibrational modes.

In pure $NdCl_3$ and $NdBr_3$ crystals, line splittings of as little as .1 cm^{-1} have been observed which can be attributed to nearest and next-nearest neighbor antiferromagnetic and ferromagnetic interactions between the Nd^{3+} ions.

Zeeman studies of $GdCl_3$:Er^{3+} and :Tb^{3+} were made both above and below the Curie temperature. The magnetic permeability at high temperatures and field strengths follows an expression derivable from a molecular field model. Below 2.2^{o} a spontaneous splitting occurs due partly, but not entirely, to the magnetic dipole field in the ferromagnetic domain.

Trivalent rare earth spectra in CaF_2 are complicated by the presence of sites of different symmetry. By rotating the crystals

in fields of up to 38,000 gauss and studying the variation of the Zeeman spectra, it is possible to deduce site symmetries. Most of the rare earths have been studied in type II CaF_2, with spectral lines from ions in tetragonal sites being most frequently observed.

When Eu^{2+} is placed in trivalent $LaCl_3$, color centers can be produced by uv radiation. The appearance of these color centers coincides with the ionization of Eu^{2+} to Eu^{3+}. Further, the color centers show polarization with respect to the C_3 axis indicating a site of high symmetry.

Crystal field parameters are given for Er^{3+} in $GdCl_3$, $LaCl_3$, $LaBr_3$, YGaG, LuGaG, and YCl_3.

Energy transfer from S to R and C to B have been studied in $LaCl_3$:Nd^{3+}. Phonon-induced relaxation rates have been determined from measurements on the radiative and pair processes. C to B transfer shows a strong temperature dependence.

The absorption spectra after flash excitation of transition metal ions in crystals are being studied. Both absorption from metastable excited states and other processes probably associated with charge transfer phenomena are observed.

---

* This research was partially supported by the U. S. Atomic Energy Commission; National Aeronautics and Space Administration under Grant NsG 361; U. S. Army Research Office, Durham; and the Air Force Office of Scientific Research, Office of Aerospace Research, United States Air Force, under AFOSR contract number AF 49 (638)-1497.

** Alfred P. Sloan Foundation Fellow

I. INTRODUCTION

The following is a composite of the recent work of the Laboratory. Much of it is that of students who began their problems under the guidance of G. H. Dieke and received their degrees within the following year. Seven of these concerned crystal spectra and the related free ion analyses; individual credits will be indicated in appropriate places below. Greater details can be found in the respective theses or subsequent publications.

Until recently, the highest resolution work except for special interferometric problems was done on a 21-foot Paschen. This still is used for the bulk of the crystal work, as the spectrum lines are not usually sharp enough to require higher resolution, but there have been several situations where the higher power of the new five-meter plane grating spectrograph has been needed. Some examples are given below.

A plan drawing of the five-meter, two-mirror system is shown in Figure 1. At the shortest wavelengths near 1200 Å (50th order) the spectral coverage is complete, the span being also about 1200 Å for the equivalent first-order wavelengths. The predisperser system consists of a concave mirror and a small plane grating. A choice of grating spacings of 300, 600, 1200 or 3600 grooves/mm can be made, depending on the degree of separation of the orders required. The vacuum ultraviolet region has been used mostly for the free ion metal spark spectra, a portion of a typical photograph of which is shown in Figure 2.[1] For longer wavelength studies narrow-band interference filters are often used in place of the predisperser system.

II. COMPARISON OF CRYSTAL AND FREE ION ENERGY LEVELS

Transitions between the $4f^n$ levels are not observable for the free ions and these levels must therefore be found by combinations with configurations of opposite parity such as the $4f^{n-1}5d$. Some of these results for the divalent and trivalent ions have recently become available, and comparisons with crystal levels can now be made.

The complete Stark manifolds for the 4f ^2F levels of Ce^{3+} in $CeCl_3$ have recently been reported by Hellwege and Hüfner[2]. They find a separation between the centers of gravity of 2215 cm^{-1}, to be compared with 2253 found by Lang[3] for the free ion. This indicates a contraction of some 1.7 percent for the 4f spin-orbit interaction.

The effect of the crystal field on the Slater parameters can be deduced from the more complex configurations. The recently reported results[4,5] for Pr^{3+} are given in Table I. Only data for complete Stark manifolds are given except the parenthetical ones where the position of a missing component could be estimated by a crystal field calculation. A contraction of several percent is indicated for the Slater parameters.

Preliminary results for the Nd^{3+} free ion[6] show a much smaller effect. So far only the ^4I levels have been found, but they correspond to within .5 percent of the crystal centers. A more detailed example is given in Table II[1] for Er^{3+}, including the Stark component positions of several important erbium-doped crystals.

The divalent ion comparisons cannot be made in such a comprehensive way because the strong low-lying $4f^{n-1}$ 5d absorption bands mask many of the $4f^n$ levels. The most detailed case is for Sm^{2+}, shown in Table III.[7] The ^7F levels are also given for the $4f^6\,6s^2$ configuration of neutral Sm to show the remarkably small difference in their spin-orbit coupling. This was very useful in the search for the Sm^{2+} levels.

TABLE I

Pr^{3+} ENERGY LEVELS

	Free Ion	LaF_3	PrES	$LaCl_3$	$CeCl_3$	$PrCl_3$	$NdCl_3$	$GdCl_3$	$LaBr_3$	YCl_3
$^3H_4$	0	0	(0)	0	0	0	0	0	0	0
$^3H_5$	2 152.09	2 163		118.7						106
$^3H_6$	4 389.09	4 264		307.3						132
$^3F_2$	4 996.61	5 015		848.1		851.20				802
$^3F_3$	6 415.24	6 355	(6 216.0)	248.1						173
$^3F_4$	6 854.75	6 831	(6 702.3)	684.2						612
$^1G_4$	9 921.24	9 797	(9 684.0)	703.7						
$^1D_2$	17 334.39	16 646	(16 731.2)	640.56	632.08	619.76	615.35	596.	596.	456
$^3P_0$	21 389.81	20 725	(20 551.3)	385.43	369.65	357.44	346.50	315.93	282.34	214
$^3P_1$	22 007.46	-	(21 148.6)	987.03	970.57	958.50	037.84	916.89	886.42	831
$^1I_6$	22 211.54	-	(21 401.6)	327.1						076
$^3P_2$	23 160.61	22 554	(22 304.5)	142.06	125.26	112.43	102.08	067.	042.26	867
$^1S_0$	50 090.29	46 700		48 710.						

TABLE II

Er^{3+} ENERGY LEVELS

Group		Free Ion	LaF_3	CaF_2	Er E.S.	$ErCl_3 \cdot 6H_2O$	$GdCl_3$	$LaCl_3$	$LaBr_3$	YGG	YCl_3	Y_2O_3
$^4I_{15/2}$	Z 1		-218.6	-218.7	-147.1	-147.3	-111.89	-108.04	-89.16	-254.79	-126.35	-202.5
	2		-167.4	-197.7	-103.1	-130.5	-73.79	-70.13	-60.20	-210.76	-104.09	-163.5
	3		-97.4	-185.9	-72.4	-110.6	-47.75	-43.77	-28.96	-205.61	-102.20	-126.5
	4		-18.9		-36.9	-22.3	-17.43	-11.52	-21.55	-178.98	-65.52	-113.5
	5		0.8	12.1	25.5	31.7	7.61	5.66	5.24	167.45	-60.11	-44.5
	6		95.2	184.3	68.7	67.3	36.11	33.56	28.19	175.75	130.20	55.5
	7		181.7	217.7	108.9	149.8	80.61	73.00	65.64	234.81	162.91	287.5
	8		224.3	233.0	156.9	161.6	126.51	121.27	100.79	272.16	165.18	307.5
	Mean	0.0	0.0		0.0	0.0	0.00	0.00	0.00	0.00	0.00	0.0
$^4I_{13/2}$	Y 1		6385.9	6354.2			6438.26	6441.47	6442.82	6317.61	6377.82	6307.5
	2		410.3	383.3			451.68	6457.58	449.64	324.66	399.15	339.5
	3		452.3	466.0			458.61	466.07	454.19	343.03	401.05	385.5
	4		482.3	498.1			474.65	479.57	476.21	532.92	411.05	391.5
	5		504.1	528.5			482.31	482.55	477.49	549.74	555.29	481.5
	6		524.1	595.8			510.64	507.81	501.80	597.75	558.78	637.5
	7		606.1				539.01	535.95	523.84	601.76	563.94	664.5
	Mean	6485.9	6480.9				6479.31	6481.57	6475.14	6466.78	6466.84	6450.2
$^4I_{11/2}$	A 1		10083.1	10070.0	10099.08	10052.1	10093.03	10099.42	10088.93	10012.22	10048.03	9990.5
	2		093.2	111.6	099.98	091.6	095.31	101.13	092.34	019.16	054.87	10011.5
	3		113.1	188.1	101.01	106.8	100.36	102.49	105.74	108.19	056.03	041.5
	4		127.3	194.3	102.71	116.3	110.55	114.00	111.74	119.08	079.50	061.5
	5		141.9		125.35	139.0	114.27	118.67	120.94	137.66	092.64	158.5
	6		179.7		150.07	148.7	129.83	132.55		142.47	112.48	176.5
	Mean	10123.6	10123.1		10113.03	10109.1	10107.23	10111.38		10089.80	10073.93	10073.3
$^4I_{9/2}$	B 1		12201.1	12581.1	12279.1	12245.1	12278.44	12284.66	12286.24	12056.24	12215.45	12121.5
	2		300.8		292.8	282.0		289.88	286.93	280.16	264.39	233.5
	3		376.1		377.9	342.5		360.16	347.20	311.18	374.14	309.5
	4		402.1		393.1	416.1		383.47	359.69	461.25	394.70	373.5
	5		473.4		490.6	460.1		439.66	414.30	491.19	396.58	401.5
	Mean	12345.5*	12350.7		12366.7	12349.2		12351.57	12338.87		12329.05	12297.9
$^4F_{9/2}$	D 1		15172.2	15172.8	15158.9	15118.7	15121.12	15143.88	15111.11	15048.03	15040.09	14917.5
	2		214.5	200.7	192.3	136.6		161.02	136.89	075.05	042.01	996.5
	3		225.7	270.8	201.4	184.1	153.76	168.52	196.23	087.46	122.64	15077.5
	4		256.8		230.1	195.3	183.43	195.82	170.99	219.50	128.12	130.5
	5		309.4		254.5	276.6		208.63	184.31	221.93	143.45	223.5
	Mean	15182.85	15235.7		15207.4	15182.3		15175.57	15149.90	15130.39	15095.23	15071.1

* these levels uncertain

TABLE II (Con't)

Group	Free Ion	LaF_3	CaF_2	Er E.S.	$ErCl_3 \cdot 6H_2O$	$GdCl_3$	$LaCl_3$	$LaBr_3$	YGG	YCl_3	Y_2O_3
$^4S_{3/2}$ E 1		18338.4	18320.8	18314.0	18248.7	18256.11	18278.59	18246.75		18148.12	18028.5
2		368.1	403.8	340.0	319.5		302.76	274.91		168.96	115.5
Mean	18299.6 *	18353.3	18362.3	18327.0	18284.1		18290.68	18260.83		18158.54	18072.0
$^2H_{11/2}$ F 1		19046.5	19045.4	19022.2	18968.0	18967.92		18950.92	18843.85	18891.95	18835.5
2		086.3	060.4	070.0	19008.0	19004.47	19027.04	981.84	865.09	892.97	842.5
3		093.4	076.0	079.6	048.5	005.43		993.24	901.71	896.82	869.5
4		140.1		098.6	081.7	015.18	032.32	19010.82	19090.73	934.79	984.5
5		198.7		111.3	099.4	034.93	053.09	030.44	104.70	019.34	19015.5
6				142.2	129.9	059.24	070.30		109.53	058.66	040.5
Mean	19010.8			19087.3	19055.9	19014.53			18985.94	18949.09	18931.3
$^4F_{7/2}$ G 1		20434.2	20453.5	20409.3	20361.1	20374.38	20373.03	20328.27		20263.76	20143.5
2		481.7	571.9	441.0	398.6	402.12	393.19	358.58		322.62	245.5
3		512.6		475.9	428.3	430.10				332.36	308.5
4		539.9		504.0	517.3		444.13				372.5
Mean	20494.1 *	20492.1		20457.6	20426.3						20267.5
$^4F_{5/2}$ H 1		22148.0	22156.5	22108.7	22060.1	22035.80	22060.62	22011.89		21943.26	21843.5
2		153.0	169.0	123.6	073.1	055.18	066.52	020.84		953.58	869.5
3		184.6		133.0	101.3		075.69	032.47		978.68	969.5
Mean	22181.8 *	20161.9		22121.8	22078.2		22067.61	22021.73		21958.51	21894.2
$^4F_{3/2}$ I 1		22464.7		22437.7	22411.1	22372.60	22395.84	24351.18		22320.77	22124.5
2		524.0		484.5	461.7	404.55	422.84	383.14		343.18	290.5
Mean	22453.9 *	22494.4		22461.1	22436.4	22388.58	22409.34	24369.16		22331.98	22207.5
$^2H_{9/2}$ K 1		24382.0		24434.8	24381.6	24383.03	24394.89	24347.04		24289.87	24161.5
2		461.5	457.0	457.0	403.9	392.47	403.67	355.28		341.86	282.5
3		533.6		514.0	470.7	403.38	414.56	408.07		344.11	319.5
4		617.9		540.0	520.9	443.14	461.66	434.16		403.04	351.5
5		638.9		632.2	544.1	477.43	494.65			421.66	405.5
Mean	24475.15	24526.8		24515.6	24464.2	24419.89	24433.89			24360.13	24304.1

* these levels uncertain

TABLE II (Con't)

Group		Free Ion	LaF_3	CaF_2	Er E.S.	$ErCl_3 \cdot 6H_2O$	$GdCl_3$	$LaCl_3$	$LaBr_3$	YCl_3	Y_2O_3
$^4G_{11/2}$	L 1		26283.6	26257.0	26289.4	26210.0	26188.56	26223.08	26125.18	25995.82	25888.5
	2		306.8	307.2	325.3	227.5	212.11	246.61	140.15	999.47	912.5
	3		335.0	321.3	334.6	276.2		249.30	166.71	26001.50	26004.5
	4		363.2	425.9	365.0	324.2	233.65	259.04	211.03	082.96	185.5
	5		432.0		370.8	346.1	255.34	277.86	217.15	245.45	196.5
	6		490.4		406.0	401.1	283.57	372.42	219.96	300.18	256.5
Mean		26376.9	26368.5		26348.5	26297.5		26271.39	26180.03	26104.23	26074.0
$^2G_{9/2}$	M 0		27384.1	27331.2		27259.8	27202.69	27238.10	27144.22	27081.14	
	1		397.1	373.6		264.6		253.30	156.21	118.80	
	2		408.5			283.9		259.32	162.36	128.32	
	3		422.3			294.2		262.11	166.24	160.73	
	4		449.0			322.9			167.55	230.92	
Mean		27319.2	27412.2			27285.1			27159.32	27143.98	
$^2K_{15/2}$	N 1		27609.7	27451.1		27335.0		27493.28		27411.57	
	2			466.7		600.1		515.91		498.96	
	3			502.4		669.2					
	4					672.2					
	5					705.2					
	6					709.8					
	7					736.6					
	8					764.8					
Mean		27584.7				27649.1					
$^2G_{7/2}$	O 1		28022.4			27916.7				27667.04	
	2		034.5			923.8				672.19	
	3		119.5								
	4		149.7			951.3					
Mean		27825.0	28081.5								
$^2P_{3/2}$	P 1		31471.6	31449.9			31334.23	31366.22	31279.07		31086.5
	2		530.4	560.5				403.64	290.20		285.5
Mean		31414.4 *	31501.0	31505.2				31384.93	31284.64		31186.0
$^4G_{7/2}$	R 1		33936.9						33699.39		33566.5
	2		975.9								646.5
	3		34005.3								727.5
	4		060.8								849.5
Mean		33849.13	33994.7								33697.5

* these levels uncertain

TABLE III

$4f^6$ Energy Levels *

	a	b	c	d	e	e	e	f	g	h
	Free Ion		Sm^{2+} in							Eu^{3+} 20 p.c. (reduced)
	Sm III	Sm I	BaClF	$LaCl_3$	$CeCl_3$	$GdCl_3$	$LaBr_3$	SrF_2	K Cl	
$^7F_0$	0.00	0.00	0	0	0	0	0	0	0	0
$^7F_1$	293.45	292.58	284.7	288.73	288.69	289.14	289.81	263	288.1	297
$^7F_2$	813.55	811.92	809.6	808.88	808.07	(807.7)	805.51	806	792.0	830
$^7F_3$	1492.66	1489.55	1489.6	1485.17	(1485.2)		1481.27	1505	(1481.)	1510
$^7F_4$	2277.88	2273.09	(2270.)	2268.60				(2335)	(2283.)	2286
$^7F_5$	3131.54	3125.46	(3114.)	3117.97				(3090)	(3149.)	3127
$^7F_6$	4026.99	4020.66	(3890.)	(4030.)				(4053)	(3979.)	
$^5D_0$			14532.8	14448.72	14421.63	14340.97	14442.48	14616.	14507.9	13814
$^5D_1$			15870.5	15781.52	(15749.)					15223
$^5D_2$			17814.5							17205
$^5D_3$			20110.							

* Numbers in parentheses are estimates for incomplete crystal Stark manifolds.

a. See reference 7.
b. W. Albertson, Phys. Rev. 52, 644 (1937).
c. Z. J. Kiss and H. A. Weakliem, Phys. Rev. Letters 15, 457 (1965).
d. G. H. Dieke and R. Sarup, J. Chem. Phys. 36, 371 (1962).
e. G. H. Dieke, unpublished.
f. D. L. Wood and W. Kaiser, Phys. Rev. 126, 2079 (1962).
g. W. E. Bron and W. R. Heller, Phys. Rev. 136, A1433 (1964).
h. G. L. Ofelt, J. Chem. Phys. 38, 2171 (1963).

Some HoIII levels are also known,[8] but the $^4I_{15/2} - {}^4I_{13/2}$ separation in CaF_2 (~ 5100 cm^{-1}) is the only divalent crystal information available[9]; it is 5438 cm^{-1} in the free ion.

The $4f^{n-1}$ bands are so broad in crystals that it is not easy to make the correlation with the free ion levels. E. Loh[10] has measured the absorption in the ultraviolet of CaF_2 doped with trivalent rare earths and finds relatively narrow bands for Ce^{3+} and Pr^{3+} at 32,500 and 45,600 cm^{-1} respectively. The corresponding lowest free ion levels are at 49,737[3] and 61,171[4,5] giving a shift of about 16,000 cm^{-1}. The right side elements present more of a problem. The lowest absorption band for Er^{3+} reported by Loh is at 64,200 cm^{-1}; the lowest free ion level is actually lower: 52,481 cm^{-1}. However, this is a sextet and transitions to the ground state $^4I_{15/2}$ are not observed. The lowest levels from which transitions of consequence occur begin at 68,352 cm^{-1}, only about 4150 cm^{-1} higher than the CaF_2 position.

If one keeps the rule that the spin selection rule is obeyed, the results for the divalent ions, however, are reasonably consistent, as shown in Table IV. (All energies are in cm^{-1})

TABLE IV

Comparison of Divalent Crystal 5d Bands with Free Ion Levels

		Free Ion	
R^{2+}	Crystal[9]	Permitted	Lowest
Ce	--	3277	3277[11]
Pr	3000	12847	12847[12]
Sm	14100	27886	26990[7]
Ho	10800	25699	18033[8]
Yb	28000	39721	33386[13]

The average difference between columns 2 and 3 is about 12,000 cm^{-1}.

III. HIGH RESOLUTION CRYSTAL STUDIES

Ho in $LaCl_3$ Some of the sharpest lines yet observed have been in .1 percent Ho^{3+} in $LaCl_3$, but in the same crystal some extremely broad ones also occur, as shown in Figure 3[14]. Tests on the five-meter spectrograph with a mercury discharge indicate a resolving power in the blue of about 600,000[15], or .04 cm^{-1}. Figure 4 (top curve) shows a densitometer trace of the hyperfine structure of the J_1 line, which is at least as sharp as the instrument can resolve. A similar test on the D_1 line in the red, where the resolution is closer to the theoretical limit of .024 cm^{-1}, shows an estimated half width of .03 cm^{-1}.

Two of the hyperfine components of the J_1 line show an unsymmetric broadening at zero magnetic field which Dieke took as an indication of the presence of the hitherto missing M = 0 line to which he gave the label J_0[14]. If a magnetic field is applied, this coincidence no longer occurs and all lines become equally sharp. However, at a field of 11,600 gauss, the pattern becomes complicated again, as shown in the lower curve of Figure 4. As other spectrum lines remain sharp at this field, this cannot be an effect of the ground state, but must be that of an interference in the excited levels. This has not yet been cleared up.

Line Broadening in R. E./La Mixtures When a rare earth is mixed into a $LaCl_3$ lattice in very low concentrations, the spectrum lines are generally sharp, but as the concentration is increased, the constitution of the surrounding ions becomes statistically uncertain, and as the ion sizes differ, the resulting crystal perturbation will vary. This will be greatest at about 50 percent concentration. Figure 5 shows such a line of Nd^{3+}.[16] For 100 percent $NdCl_3$ the lines again are sharp, but other effects appear (see below). Figure 6 shows the concentration dependence of the Pr^{3+} spectrum in mixtures with $LaCl_3$. Careful high resolution studies of line width show that the lines have a Gaussian shape rather than Lorentzian and E. S. Dorman has developed a statistical theory which can account for this.[17] The pure $PrCl_3$ crystals also show extensive pair spectra.[18] Transition probabilities have also been determined by numerical integration of high resolution photoelectric absorption curves.[17]

Vibronic Side Bands Figure 6 also shows the development of an extensive series of more or less diffuse lines as the concentration is increased. A similar effect is seen for pure $NdCl_3$ in Figure 7. These vibronic side bands which accompany the strong electronic rare earth spectral lines give information on the phonon frequencies of the crystal and their interactions with different electronic levels of the rare earth ion. Because of the relatively high symmetry of the $LaCl_3$ type lattices (p63/m) and the low number of atoms per unit cell (8), this is a particularly attractive system to study.[19,20] In trichloride lattices it is found that Nd^{3+} and Pr^{3+} give relatively strong vibronics.

The system chosen for discussion here is 1 percent Pr^{3+} in $NdCl_3$, wherein it is possible to compare impurity vibronic frequencies with those of the main constituent. The transitions from $^4I_{9/2}$ ($\mu = \pm 5/2$) to $^2P_{1/2}$, $^2D_{5/2}$ and $^2P_{3/2}$ of Nd^{3+} and $^3H_4$ ($\mu \pm 2$) to $^3P_0$ and $^3P_2$ of Pr^{3+} were studied in absorption at 4.2°K using magnetic fields up to 30,000 gauss. The vibronic spectrum is polarized and shows the same Zeeman splitting as the main line. The lines are quite narrow ranging from 1 to 10 cm^{-1}. Figure 7 shows the $^4I_{9/2}$ ($\mu = \pm 5/2$) to $^2P_{1/2}$ transition of $NdCl_3$.

Of the vibronic lines which are common to both Nd^{3+} and Pr^{3+}, there are no observable shifts in the vibronic frequencies to within $\pm$ 1 cm^{-1}, indicating both the Nd^{3+} and Pr^{3+} ions are perturbed by phonons of the same frequency. Table V shows the phonon frequencies obtained from the vibronics accompanying the electronic transition $^4I_{9/2}$ ($\mu = \pm 5/2$) to $^2P_{1/2}$ of $NdCl_3$ and $^3H_4$ ($\mu = \pm 2$) to $^3P_0$ of 1 percent Pr^{3+} in $NdCl_3$.[21] All measurements are at zero magnetic field and have an accuracy of better than one cm^{-1}.

The frequencies of the observed Raman active phonons are also given.[21] The number of frequencies listed is much larger than that predicted by assuming interaction only with $\vec{k} = 0$ phonons (16). Both multiphonon processes and other points of high symmetry in the Brillonin zone must be considered in a further analysis. The agreement of the phonon frequency of many of the Pr^{3+} and Nd^{3+} vibronics gives a basis for using a single ion analysis for Nd^{3+}. Using this approximation, the polarization selection rules for Nd^{3+} were derived and are being used for analyzing the spectra.

TABLE V

Phonon frequencies for Pr^{3+} and Nd^{3+} in $NdCl_3$*

	Nd^{3+}		Pr^{3+}		
$\nu(cm^{-1})$	π	σ	π	σ	Raman Spectrum
6.6	x				
14.2	x				
20.5	x				
73.4	x				
77.5	x			x	
81.5				x	
83.6	x				
92.2	x				
98.4	x			x	
104.4	x			x	104
110.5	x			x	
114.4		x			
119.7		x			
123.4		x		x	
129.5	x	x	x	x	
135.1		x			
138.5	x	x			
141.0				x	
154.6				x	
155.6	x	x			
156.3			x		
160.5	x	x	x		
166.2	x	x	x		
169.8				x	
172.3	x			x	
181.3	x	x		x	
186.8		x			
187.6	x				183
188.5				x	
192.5	x	x			191
194.1				x	
196.8		x			
201.1	x	x			
202.3				x	
205.4	x	x			
209.7				x	
210.3	x				
217.1	x			x	217
223.3		x			224
234.2		x			
237.7				x	
254.5	x			x	

* Observation of a transition is indicated by an x. Bracketed frequencies may be the same.

Exchange Effects in $NdCl_3$ and $NdBr_3$ The absorption spectra of single-crystal samples of pure $NdCl_3$ and $NdBr_3$ have been obtained at low temperatures (4.2° to $1.2^{\circ}K$) under high resolution in the region from 2700 Å to 1 μ for $NdCl_3$ and in the region 3000 A to 7000 Å for $NdBr_3$[23]. Aside from small shifts in the Stark multiplets of the order of 20 cm^{-1} (see Figure 8) the principal difference from the spectrum of 1 percent $NdCl_3/LaCl_3$ is that each line is accompanied by two symmetrically placed satellites of comparable intensity, one on either side of the main line. Zeeman studies were made of the lines in fields up to 36 kilogauss, applied both parallel (see Figure 9) and perpendicular to the axis which joins the nearest-neighbor Nd^{3+} within the sample. The sources of these additional lines are interactions coupling neighboring Nd^{3+} ions. Only a small part of this coupling is attributable to known, calculable interactions between the ions -- electric dipole, magnetic dipole, and electric quadrupole. A satisfactory interpretation of the spectra can be obtained by assuming an additional coupling between Nd^{3+} neighbors i and j of the form $\mathcal{H}_{ij} = \mathcal{J}_{ij} S_{zi} S_{zj}$ where S_z is the z component of fictitious spin 1/2. This coupling is assumed to be due to electron exchange.

The sign and magnitude of the nearest-neighbor coupling has been obtained for the ground and five excited states in $NdCl_3$ and for the ground and two excited states in $NdBr_3$. The sign and magnitude of the next-nearest-neighbor coupling has also been obtained for the ground and two excited states in $NdBr_3$ (see Table VI). Column Δ_σ and Δ_π give the measured splittings of the spectrum lines in σ and π polarizations respectively. These are sums or differences of the corresponding upper and lower state energy splittings, depending on the particular situation. These have been resolved into respective energy splittings ΔE and $\Delta E(Z_1)$ for the upper and lower states respectively. Corrections for the magnetic dipole contributions have been applied; the last column gives the residue, which is attributed to the exchange energy of near-neighbor neodymium ions.

TABLE VI

Splittings of Energy Levels (ΔE) and Spectral Lines ($\Delta_{\sigma,\pi}$)
(in units of cm^{-1})

$NdCl_3$ (n-n)

Level	Observed				Magnetic Dipole (ferro)	Non-Dipolar	
	Δ_σ	Δ_π	ΔE	$\Delta E(Z_1)$	ΔE	ΔE	Coupling
Z_1^*				0.70 ± 0.03	0.11	0.81	a-f
B_2	0.96 ± 0.07	0.33 ± 0.08	0.32 ± 0.08	0.65 ± 0.08	0.21	0.53	a-f
B_4	0.52 ± 0.02	0.88 ± 0.02	0.18 ± 0.02	0.70 ± 0.02	0.04	0.14	f
G_1	0.71 ± 0.04	0.76 ± 0.02	0.02 ± 0.02	0.73 ± 0.03	0.03	0.01	a-f
I_2	0.74 ± 0.01	0.62 ± 0.02	0.06 ± 0.02	0.68 ± 0.02	0.04	0.10	a-f
K_1	0.88 ± 0.02	0.55 ± 0.05	0.33 ± 0.04	0.72 ± 0.04	0.03	0.36	a-f

* Weighted Mean Value

TABLE VI (Con't)

$NdBr_3$ (n-n)

Level	Observed Δ_σ	Observed Δ_π	Observed ΔE	Observed $\Delta E(Z_1)$	Magnetic Dipole (ferro) ΔE	Non-Dipolar ΔE	Non-Dipolar Coupling
Z_1^*				1.02 ± 0.02	0.09	1.11	a-f
B_1	1.01 ± 0.05	1.07 ± 0.06	0.03 ± 0.06	1.04 ± 0.06			a-f
B_2	0.98 ± 0.10	1.05 ± 0.03	0.04 ± 0.10	1.01 ± 0.10			a-f
C_3	1.28 ± 0.01	0.71 ± 0.02	0.29 ± 0.02	1.00 ± 0.02	0.18	0.11	f
I_1	1.09 ± 0.03	0.96 ± 0.02	0.07 ± 0.03	1.03 ± 0.03	0.01	0.08	a-f

$NdBr_3$ (n-n-n)

Level	Observed Δ_σ	Observed Δ_π	Observed ΔE	Observed $\Delta E(Z_1)$	Magnetic Dipole (a-f)	Non-Dipolar ΔE	Non-Dipolar Coupling
Z_1^*				0.20 ± 0.01	0.01	0.21	f
C_3	0.26 ± 0.01	0.12 ± 0.01	0.07 ± 0.01	0.19 ± 0.01	0.00	0.07	a-f
I_1	0.19 ± 0.01	0.22 ± 0.01	0.02 ± 0.01	0.20 ± 0.01	0.02	0.00	—

* Weighted Mean Value

The dominant coupling between ground state ions in both crystals is an antiferromagnetic one between the near neighbors, which lie in a chain along the optic axis. The next-near-neighbors lie in neighboring chains and are ferromagnetically coupled, but at low temperatures a given ion will be surrounded by equal numbers of positive and negative spins. J. S. Marsh has shown how to apply Ising-chain statistics to such a case with reasonable success[24].

Ferromagnetic $GdCl_3$ Pure $GdCl_3$ is ferromagnetic below $2.2^{\circ}K$. Above this temperature there is no magnetic ordering, but the inter-ionic interaction is strong enough to cause a broadening of the line due to the individual sites being no longer magnetically equivalent. If a strong enough magnetic field is applied, however, the ground state spins are forced into alignment. Absorption lines from the lowest magnetic state ($M = -7/2$) now are again sharp, as is shown in Figure 10[21]. The extra line which appears in the highest field is due to a forbidden transition which becomes mixed with a permitted one due to a crystal Paschen-Bach effect.

Crystals of $GdCl_3$ with 1 percent Er and Tb have been studied above and below the Curie temperature ($2.2^{\circ}K$) at fields of up to 36 kilogauss in order to measure the internal magnetic fields for various conditions[25]. At higher temperatures, the line splitting is consistent with a permeability and magnetization given by the expressions

$$u_z = 1 + 4\pi M_z / H_z$$

$$M_z = .1925\, B_{7/2} \left[(H_z + 16.21\, M_z)\, \beta\, g / kT \right]$$

for magnetic fields parallel to the crystal axis. $B_{7/2}(x)$ is the Brillouin function

$$B_{7/2}(x) = 4 \coth(4x) - 1/2 \coth(x/2)$$

β the Bohr magneton, and g the spectroscopic splitting factor. For large enough perpendicular fields H_x the magnetization is approximated by

$$M_x = .1925\, B_{7/2}\left[\beta g H_x / kT\right]$$

Below the Curie temperature a spontaneous splitting is observed with no applied field. At applied fields above the saturation point for M_z a linear differential splitting is observed. The resulting splitting factors are not entirely consistent with the higher temperature values and may contain a contribution due to Er - Gd exchange.

Zeeman Studies for Nonequivalent Sites In some crystals such as the garnets, there are ion sites which are equivalent insofar as the crystal field is concerned but when a magnetic field is applied, it does not have the same relation to all ions. Thus, several Zeeman patterns are observed simultaneously. If the field is chosen parallel to a local axis of symmetry for one ion, it will in general not be right for others, but a few selected directions can be found so that the individual splitting factors can be interpreted. This situation was encountered first in paramagnetic resonance experiments[26], but can also be used to give information on excited states. Figure 11 illustrates the results for absorption to the lowest component of the $^2F_{5/2}$ manifold of Yb^{3+} in YAG. The resulting splitting factors as well as other levels derived from absorption and fluorescence experiments are given in Table VII.

TABLE VII

Zeeman Splitting Factors for Er^{3+} in Garnets

State	Energy	Yttrium Aluminum Garnet s_x	s_y	s_z
$^2F_{7/2}(\Gamma_7)$	0.0	3.87	3.78	2.47
(Γ_6)	612.2	-	-	-
$^2F_{5/2}(\Gamma_7)$	10324.6	1.27	2.46	0.49
(Γ_8)	10610.	-	-	-
	10670.	-	-	-

State	Energy	Yttrium Gallium Garnet s_x	s_y	s_z
$^2F_{7/2}(\Gamma_7)$	0.0	3.73	3.60	2.85
(Γ_6)	544.2	-	-	-
$^2F_{5/2}(\Gamma_7)$	10312.76	1.80	1.98	0.35
(Γ_8)	10586.7	-	-	-
	10739.3	-	-	-

Charge Compensation of Rare Earth Ions The spectra of trivalent rare earth ions in alkaline earth fluorides is complicated by the fact that the trivalent ion replaces a M^{2+} ion. The charge compensation defects introduced influence the local environment of some of the rare earth ions, modifying the site symmetry. In type II CaF_2 (grown in an excess of fluorine), the predominate site symmetries are cubic, tetragonal and trigonal. Electron paramagnetic resonance measurements on type II $CaF_2:Er^{3+}$ indicate a relative abundance of 15:20:1, respectively. The tetragonal site is thought to be due to an interstitial F^- along a< 100 > direction.

The spectra due to all of their sites are superimposed, so that it is not possible to say without further investigation which spectral line arises from which site. (This, of course, must be decided before any further analysis can be made). Also, due to the existence of equivalent but magnetically distinguishable sites, there is no zero field polarization to aid in the interpretation of the spectra.

The problem of paramagnetic trivalent rare earth ions in nonequivalent sites has been studied by means of epr techniques. From the variation of the splitting factor as the magnetic field is rotated about a given axis, it is possible to deduce the site symmetry of the ion. C. W. Rector, using the 21-foot Paschen magnetic fields up to 38,000 gauss, has been able to develop a similar technique for the optical spectra.[27,28] The crystals are rotated and the Zeeman spectra photographed every 5^o. A composite is then assembled showing the variation with rotational angle of the Zeeman effect. Figure 12 shows a tracing of such a composite for type II $CaF_2:Nd^{3+}$. The right hand side is due to a tetragonal site with an axis along the [100] direction; the left hand side is due to a trigonal site with a [111] direction axis. The angular variations are quite different. Note particularly the 70^o - 110^o split of the turning points in the trigonal case compared with the 90^o - 90^o split in the tetragonal case. Also, note the 70^o - 110^o split of the tetragonal coalescence points. Using selection rules and the rotational patterns, it is possible to assign representations to the levels. At present, Pr^{3+}, Nd^{3+}, Tb^{3+}, Dy^{3+}, Ho^{3+}, Er^{3+} and Tm^{3+} have been studied in

varying degrees. Most of the lines studied in type II CaF_2 indicate tetragonal sites. It is interesting to note that non-Kramers salts can also be studied. At sufficiently large magnetic fields, a crystal Paschen-Bach effect occurs, decoupling certain pairs of levels from the component of the crystal field splitting them. These pseudo-Kramers' doublets then show a rotational variation much like that of a Kramers' doublet. Because of the high J value, such effects are particularly striking in Ho^{3+}, as shown in Figure 13.

A related problem is that of putting a divalent ion, Eu^{2+}, in a trivalent lattice, $LaCl_3$[29]. Although broad bands corresponding to transitions to the d levels are observed, no sharp lines appear. Rotational epr studies indicate hexagonal symmetry. When the crystals are exposed to ultraviolet light, darkening due to color centers appears. The color centers can be produced at room or lower temperatures by a source such as a mercury pen lamp and removed by mild heating. The color centers are clearly connected with the presence of Eu^{2+} since they do not appear in other doped $LaCl_3$ crystals. Plates taken on the 21-foot Paschen show the appearance of the $^7F_0$ to $^5D_2$, $\mu = 2$, absorption line of Eu^{3+} as the crystal becomes more colored, indicating a relationship between the ionization of Eu^{2+} and the production of the color centers (Figure 14).

Four absorption bands have been measured, two in π and two in σ polarization with respect to the optic axis of the crystal (Figure 15). The several bands keep a constant ratio as the crystal is bleached indicating a single type of center. Further, the polarization of the bands with respect to the C_3 axis indicates an unusual symmetry for the electron trap.

IV. CRYSTAL FIELD CALCULATIONS

Erbium-Doped Crystals Crystal field calculations have been made for several of the Er^{3+} crystals for which the energy levels are given in Table II. These are given in Table VIII. The $LaCl_3$ values are similar to those found by Dieke and Varsanyi[30], except that J-mixing has been taken into account. The two sets of garnet parameters also include J-mixing effects. A comparison of the computed and experimental levels for YGaG case is given in Figure 16. The parameter adjustment was made using the Z and Y groups only; the A group correlations are independent. Experimental data also exists for the YAG and LuA garnets but so far the agreement is not nearly so good. Further details can be found in Dieke's monograph[31].

Figure 17 shows some results of Rakestraw's[32], in which a crystal field of very low symmetry, in this case C_2, can accidently be approximated by a field of much higher symmetry, the octahedral field parameters for which are given in the last column of Table VIII.

TABLE VIII

Crystal Field Parameters for Er^{3+}

K	Q	$GdCl_3$	$LaCl_3$	$LaBr_3$	YGaG	LuGaG	YCl_3
2	0	112	96	117	-14	32	
2	2				89	58	
4	0	-45.5	-34.9	-39.6	-238	-245	175
4	2				255	175	
4	4				920	948	+875
6	0	-25.0	-25.6	-19.2	33.0	338	10.4
6	2				58	-83	
6	4				645	664	-218.4
6	6	246	249	212	-70	-48	

V. MULTIPHONON PROCESSES IN $LaCl_3:Nd^{3+}$

Previous studies [33, 34] have shown that there is a definite relationship between the energy differences to the next lowest level and the fluorescence efficiency of rare earth energy levels. In $LaCl_3$, fluorescence is not expected from levels lying less than 1000 cm^{-1} above another. However, previous studies have not delineated the competing quenching effects of ion pair processes and multiphonon emission. It has been shown by relative fluorescence intensity measurements on 3.5 percent $LaCl_3:Ho^{3+}$ that ion pair relaxation rates are on the order of radiative rates[35, 36]. In the case of E to C the range is 7.5 Å.

Lifetime and quantum efficiency studies have been conducted on the levels immediately above the $^4F_{3/2}$ level of Nd^{3+} in $LaCl_3$[37]. These levels are of interest since they may decay by nonradiative transitions involving energy transfers of from 800 cm^{-1} to 1300 cm^{-1}. The lifetime measurements used both stroboscopic techniques[34, 38] and a P.A.R. model T.D.H. -9 waveform eductor.

The lifetime of S was found to be very short, with a nonradiative quantum efficiency to R of typically 80 percent, depending on concentration and temperature. At low temperatures there are no Nd^{3+} ion pair processes possible for the transition from S to R and it is attributed to multiple phonon emission. This transition rate is 4.7×10^4 $sec.^{-1}$ at 4.2°K and is independent of concentration. At high concentration, the lifetime of S decreases by a pair process involving W, for which a near resonance exists.

The lifetime of C shows a slight concentration dependence which becomes negligible at low concentrations. The lowest concentration sample of .1 percent $LaCl_3:Nd^{3+}$ was grown from 99.999 percent pure $LaCl_3$. The transition rate from C to B is 2.2×10^3 $sec.^{-1}$ at 4.2°K and is strongly temperature dependent as shown in Table IX.

It is to be noted that at 4.2°K the S → R transition rate is appreciably greater than the C → B rate. This may be due either to the larger energy gap for the C → B process (1150 cm^{-1} as compared to 1000 cm^{-1}) or to the fact

that the C → B transition involves a spin change.

TABLE IX

Relaxation rate from C to B in a .1 percent $LaCl_3:Nd^{3+}$ as a function of temperature.

Temperature	Rate
4.02°K	2.20×10^3 sec.$^{-1}$
77	1.65×10^3
195	6.05×10^3
300	18.3×10^3

VI. EXCITED STATE ABSORPTION SPECTROSCOPY

The broad absorption bands of the transition metal ions in solids are usually observable only if the spin is the same as the ground state. However, several of the ions have metastable states with spins different from that of the ground state. If the ion is pumped into this state by an intense flash lamp, absorption from the metastable state to bands not detectable from the ground state can be measured.[39] In addition, bands due to charge transfer processes in which the ionization state is changed could also be detected.

The absorption coefficient is measured by means of a pulsed xenon short arc lamp in which the light intensity is increased by 10^2 for several microseconds. This probe light is detected by a gated photomultiplier, the total charge being stored on a capacitor and read by an electrometer. Recently, using selected lamps, it has been possible to obtain repeatability of better than $\pm$ .25 percent.

Figure 18 shows the absorption band of $Al_2O_3:Cr^{3+}$ at 3840 Å in π polarization, designated $^2T_{2g}$[40,41], at three temperatures.[42] The other polarization does not show such a variation, although taken with an apparatus of lower repeatability than that described above, the variation with temperature is considered significant.

FIGURE CAPTIONS

Figure 1. Five-meter spectrograph with plane grating predisperser in a typical setup for metal spark spectra.

Figure 2. Free ion spark spectra of erbium at various peak currents, taken on 5-meter plane grating spectrograph in 26th to 33rd order. Equivalent first order wavelengths are indicated below.

Figure 3. Different types of Ho^{3+} absorption lines. (1-4) sharp D_3' line, and D_1, D_5 and J_3 hyperfine lines, all on 5-meter; (5-10) J_3, J_5', J_5, J_6, I_1 and I_8, all on Paschen.

Figure 4. Densitometer traces of hyperfine structure of 4180 Å Ho^{3+} J_1 line in $LaCl_3$. Top: zero field; bottom: short wavelength set of Zeeman components with 11,600 gauss field.

Figure 5. Effect on concentration on line width of Nd^{3+} C group in Nd/La mixtures.

Figure 6. Effect of concentration on Pr^{3+} 4883 Å $^3P_0$ absorption line for Pr/La mixtures. The concentrations are, from top to bottom, 0.25 %, 2 %, 15 %, 50 %, 85 %, and 100 %.

Figure 7. The $^4I_{9/2}$ ($\mu = \pm 5/2$) to $^2P_{1/2}$ transition of $NdCl_3$ and its Zeeman effect. The electronic line at the right is highly over-absorbed. Some of the strong phonon lines are also over-absorbed.

Figure 8. C Group of Nd^{3+} in $LaCl_3$ and pure Nd crystals. The triple structure is due to Nd-ion exchange interactions.

Figure 9. Parallel Zeeman splitting of I_1 (π) in $NdBr_3$. Bath temperature is 1.5°K. Region shown is centered at λ_{vac} = 4241 Å and is 5 Å (30 cm^{-1}) wide.

Figure 10. Parallel Zeeman effect of Gd^{3+} A group near 3115 Å in pure $GdCl_3$ at 4.2°K (π polarization).

Figure 11. Zeeman effect of 9683 Å Yb^{3+} line in yttrium aluminum garnet showing superimposed patterns from magnetically inequivalent sites.

Figure 12. Composite showing the variation of Zeeman absorption spectra of type II $CaF_2:Nd^{3+}$ for rotation about the [110] axis. The temperature is near 4.2°K.

Figure 14. Absorption spectrum of a $LaCl_3:Eu^{2+}$ crystal at 4650 Å in σ polarization.

a. No prior irradiation, 77°K.

b. 5-minute irradiation prior to exposure at 77°K.

c. 120-minute irradiation prior to exposure at 77°K.

d. Crystal deeply colored prior to exposure at 4.2°K.

e. $LaCl_3$ crystal grown to contain predominantly Eu^{3+}. Exposure at 4.2°K.

Figure 15. Absorption spectra at 77°K in $LaCl_3:Eu^{2+}$ crystals. Color centers induced by ultraviolet radiation.

Figure 16. Observed and calculated Stark shifts of three lowest groups of Er^{3+} in yttrium gallium garnet.

Figure 17. Observed and calculated Stark shifts of four lowest groups of Er^{3+} in anhydrous yttrium chloride (octahedral approximation).

Figure 18. The $^2E \rightarrow {}^2T_{2g}$ absorption band at 3840 Å in π polarization as a function of temperature.

REFERENCES

1. W. J. Carter, Ph. D. Thesis, Johns Hopkins University (1966)
2. K. H. Hellwege and S. Hüfner, Fifth Rare Earth Research Conference, Ames, Iowa (1965)
3. R. Lang, Canada Journ. Res. A13, 1 (1935); A14, 127 (1936)
4. J. Sugar, J. Opt. Soc. Am. 55, 1058 (1965)
5. H. M. Crosswhite, G. H. Dieke, and W. J. Carter, J. Chem. Phys. 43, 2047 (1965)
6. D. J. G. Irwin, unpublished
7. A. Dupont, Ph. D. Thesis, Johns Hopkins University (1966)
8. J. H. McElaney, Ph. D. Thesis, Johns Hopkins University (1964)
9. D. S. McClure and Z. Kiss, J. Chem. Phys. 39, 3251 (1963)
10. E. Loh, Phys. Rev. 147, 332 (1966)
11. J. Sugar, J. Opt. Soc. Am. 55, 33 (1965)
12. J. Sugar, J. Opt. Soc. Am. 53, 831 (1963)
13. B. W. Bryant, J. Opt. Soc. Am. 55, 771 (1965)
14. G. H. Dieke and B. Pandey, J. Chem. Phys. 41, 1952 (1964)
15. G. H. Dieke and D. F. Heath, Japan J. Appl. Phys. 4, Suppl. 1, 455 (1965)
16. A. H. Piksis, unpublished
17. E. Dorman, J. Chem. Phys. 44, 2910 (1966)
18. G. H. Dieke and E. Dorman, Phys. Rev. Letters 11, 17 (1963)
19. I. Richman, R. A. Satten and E. Y. Wong, J. Chem. Phys. 39, 1833 (1963)
20. R. A. Satten, J. Chem. Phys. 40, 1200 (1964)
21. E. Cohen, unpublished
22. J. T. Hougen and S. Singh, Proc. Roy. Soc. A277, 193 (1964)
23. G. A. Prinz, Physics Letters 20, 323 (1966); Phys. Rev. (accepted for publication)
24. J. S. Marsh, Ph. D. Thesis, Johns Hopkins University (1966); Physics Letters 20, 355 (1966)
25. D. J. Randazzo, Ph. D. Thesis, Johns Hopkins University (1966)
26. W. P. Wolf, M. Ball, M. T. Hutchings, M. J. M. Leask and A. F. G. Wyatt, J. Phys. Soc. Japan 17, Suppl. B-I, 443 (1962)

27. C. W. Rector, Ph. D. Thesis, Johns Hopkins University (1966)

28. C. W. Rector, B. C. Pandey, and H. W. Moos, J. Chem. Phys. 45, 171 (1966)

29. B. F. Kim, unpublished

30. F. Varsanyi and G. H. Dieke, J. Chem. Phys. 36, 2951 (1962)

31. G. H. Dieke, Spectra and Energy Levels of Rare Earth Ions in Crystals, to be published by John Wiley and Sons, Incorporated

32. J. W. Rakestraw and G. H. Dieke, J. Chem. Phys. 42, 873 (1965)

33. G. H. Dieke, Low, Paramagnetic Resonance Conference, (Academic Press, Inc., New York 1963) Vol. I., p. 237

34. G. E. Barasch and G. H. Dieke, J. Chem. Phys. 43, 988 (1965)

35. J. F. Porter, Ph. D. Thesis, Johns Hopkins University (1966)

36. J. F. Porter and H. W. Moos, to be published in the Physical Review

37. W. D. Partlow, to be published

38. C. F. Hendee and W. B. Brown, Phillips Tech. Rev. 19, 50 (1957)

39. F. Gire and G. Mayer, Ann. de Radioelectricite 18, 112 (1963)

40. C. S. Naiman and A. Linz in Proceedings of the Symposium on Optical Masers, New York 1963, Polytechnic Press (1963) p. 369

41. M. Shinada, S. Sugano and T. Kushida, Tech. Rep. of ISSP A, No. 196 (April 1966)

42. J. Huang, to be published

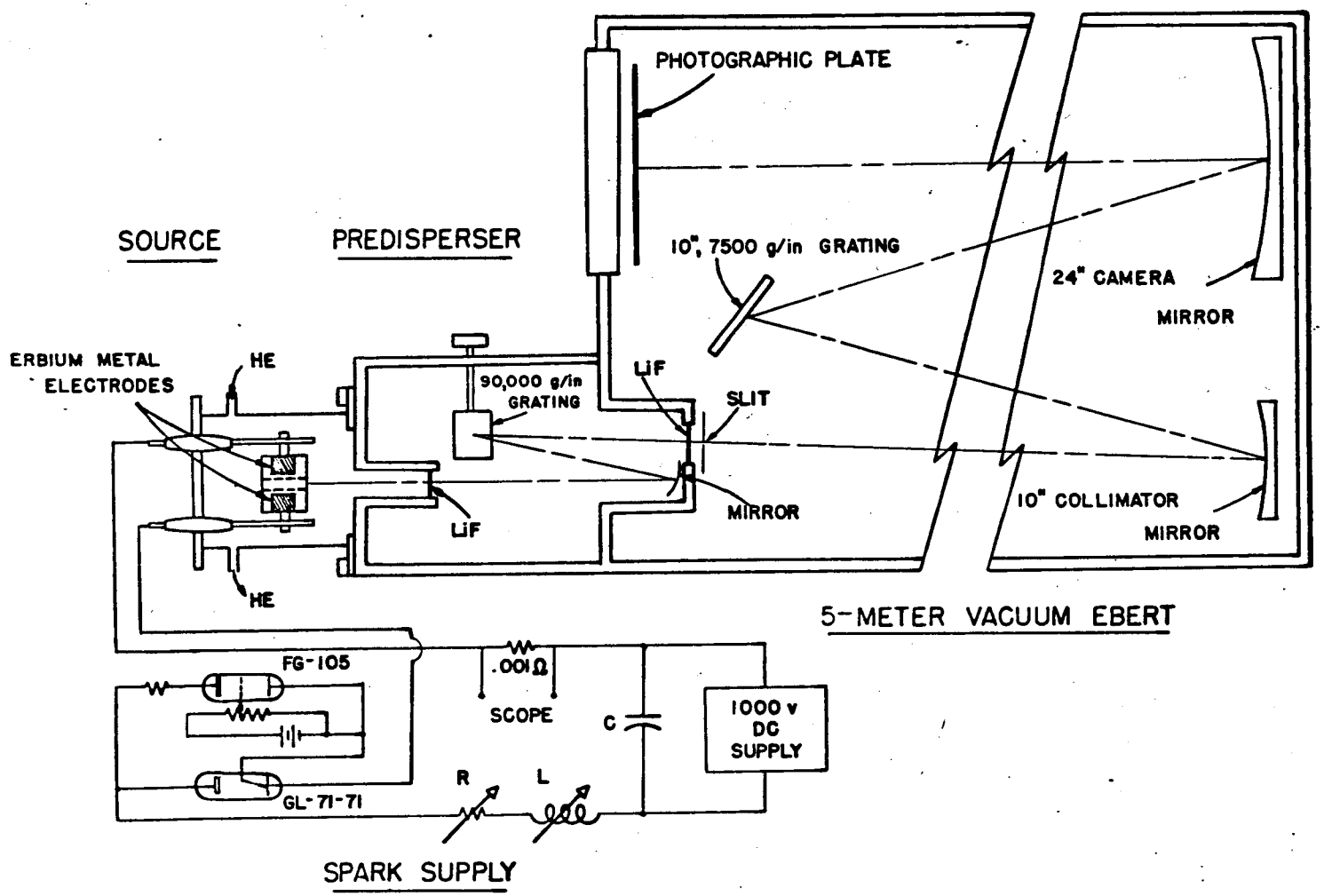
PHOTOGRAPHIC PLATE
SOURCE
PREDISPERSER
10", 7500 g/in GRATING
24" CAMERA MIRROR
ERBIUM METAL ELECTRODES
HE
90,000 g/in GRATING
LiF
SLIT
LiF
MIRROR
10" COLLIMATOR MIRROR
HE
5-METER VACUUM EBERT
FG-105
.001Ω
SCOPE
C
1000 v DC SUPPLY
R
L
GL-71-71
SPARK SUPPLY

Figure 1

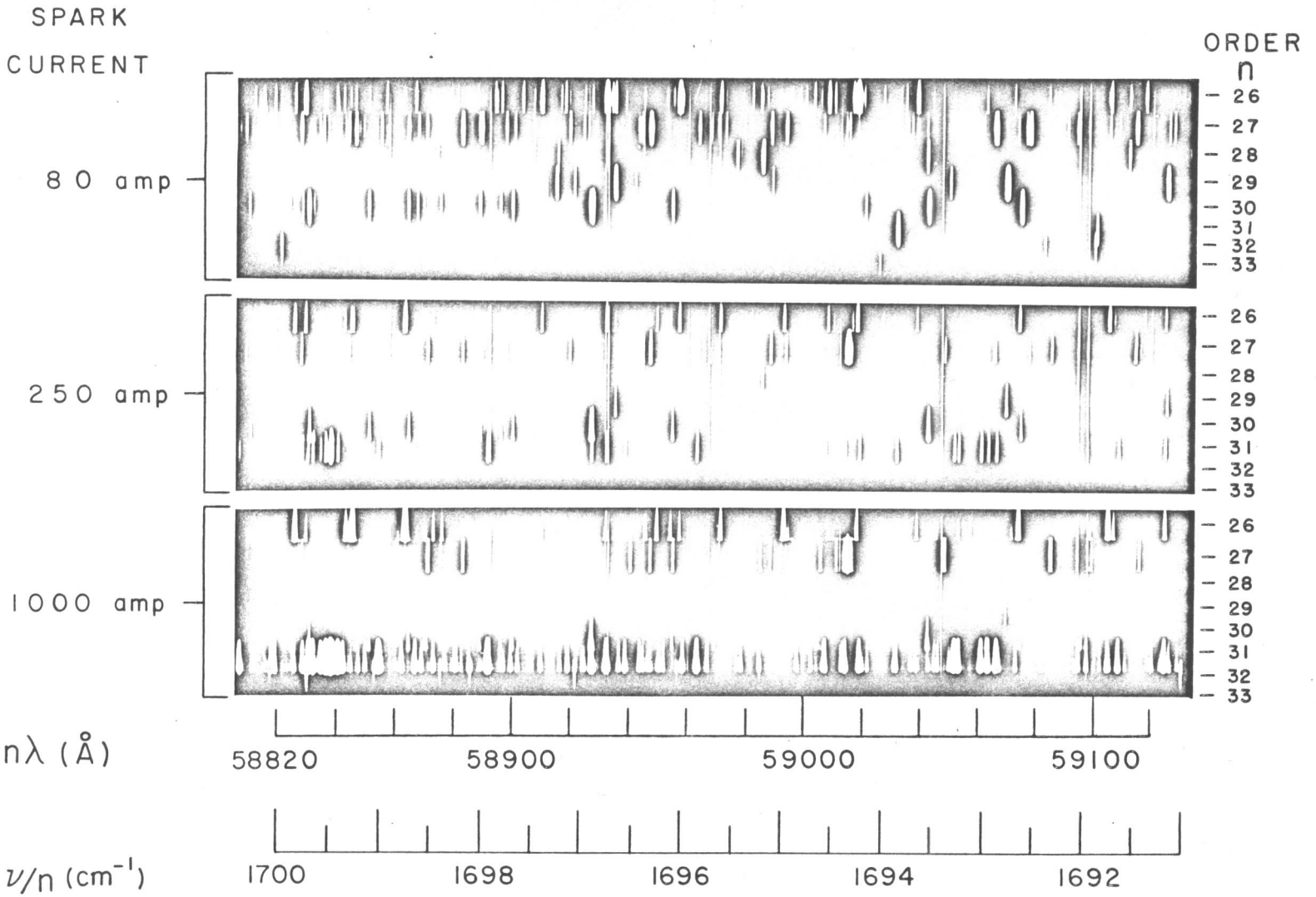
SPARK
CURRENT
ORDER
n
80 amp
250 amp
1000 amp
26
27
28
29
30
31
32
33
nλ (Å)
58820
58900
59000
59100
ν/n (cm⁻¹)
1700
1698
1696
1694
1692

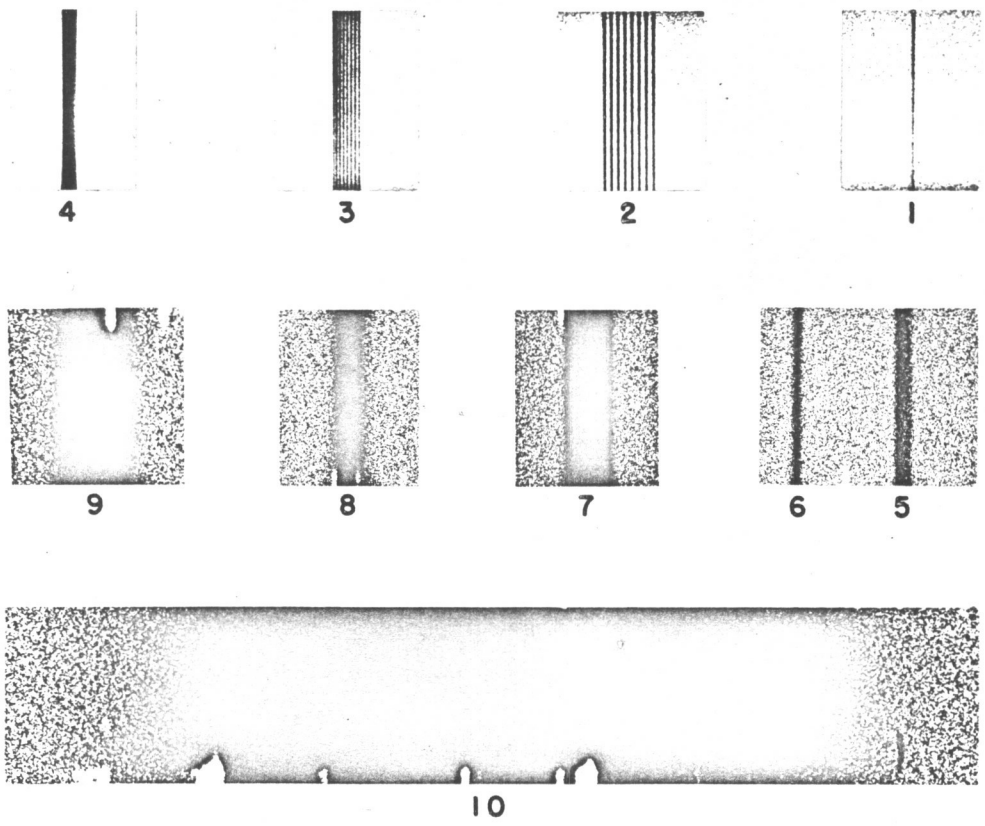
4
3
2
1
9
8
7
6
5
10

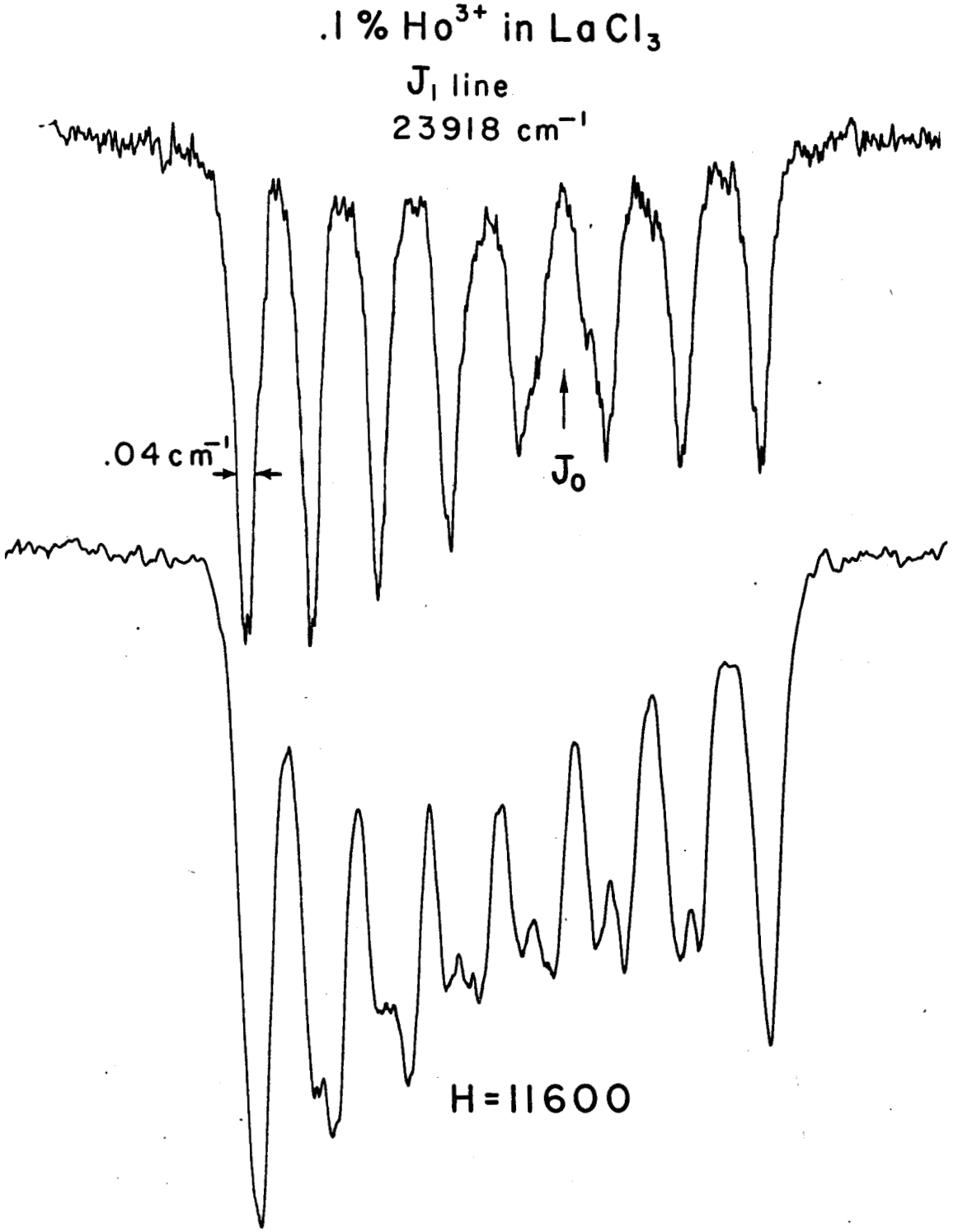
.1 % Ho^{3+} in $LaCl_3$
J_1 line
23918 cm^{-1}
.04 cm^{-1}
J_0
H=11600

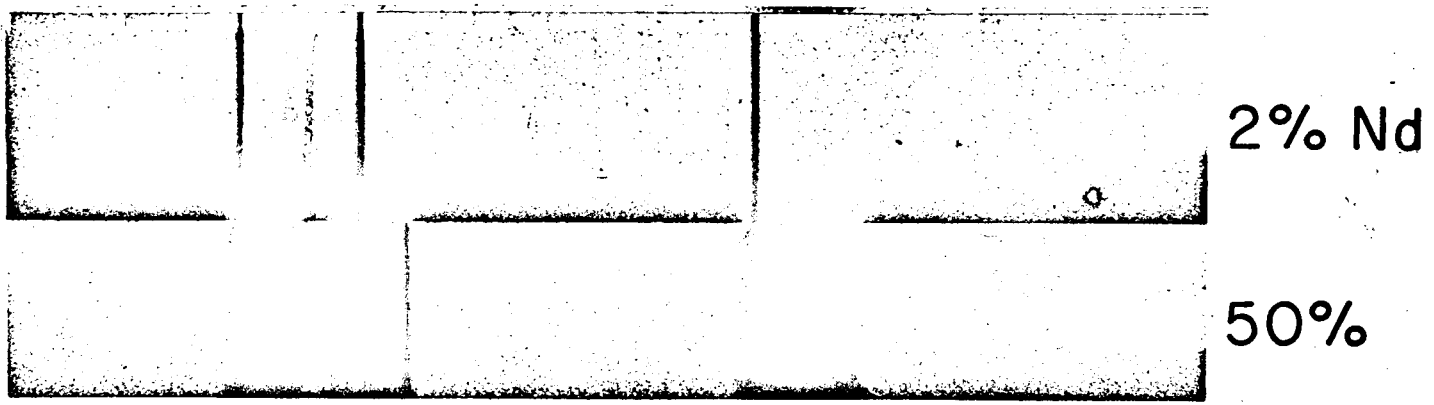

$NdCl_3$ in $LaCl_3$

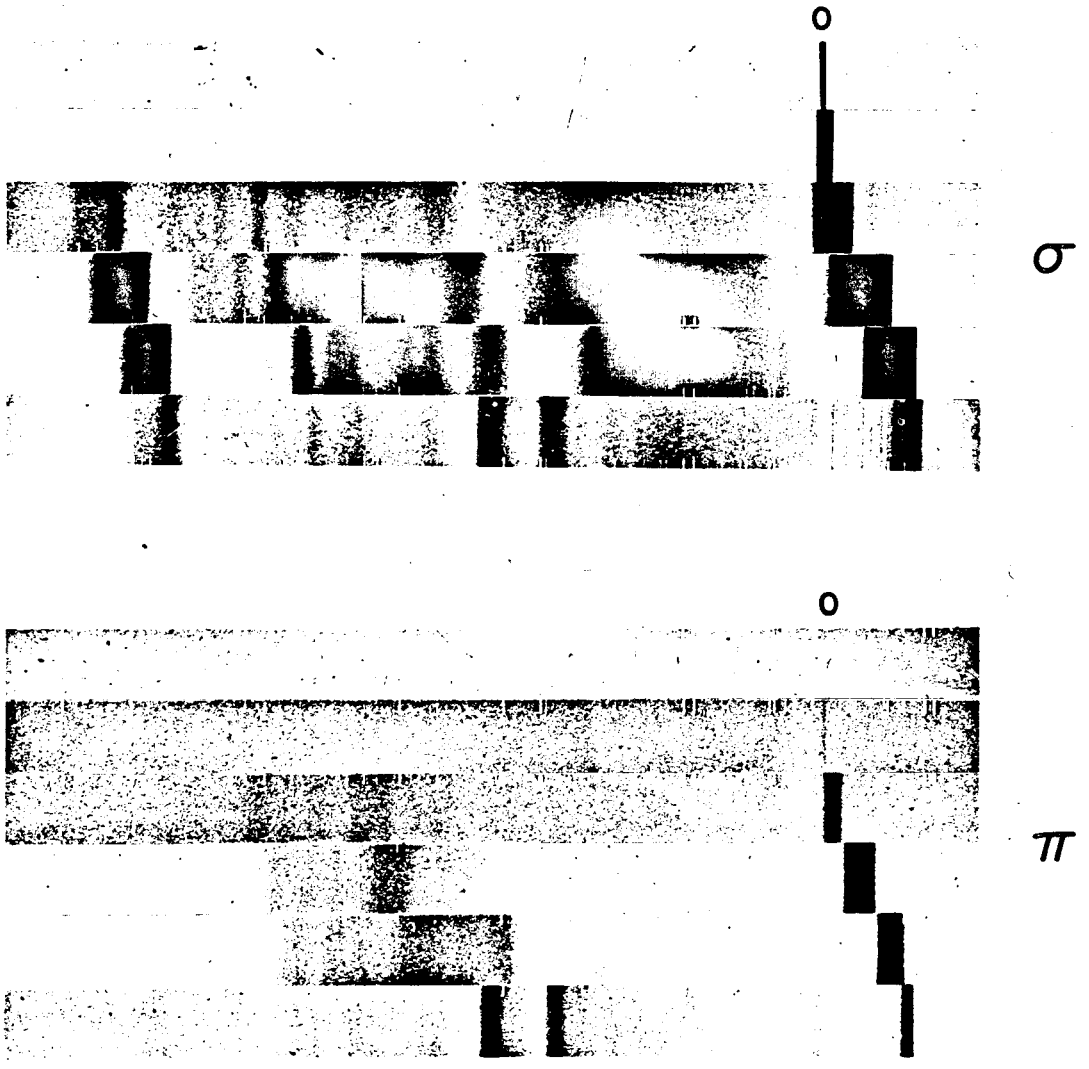
0
σ
0
π

$NdCl_3$

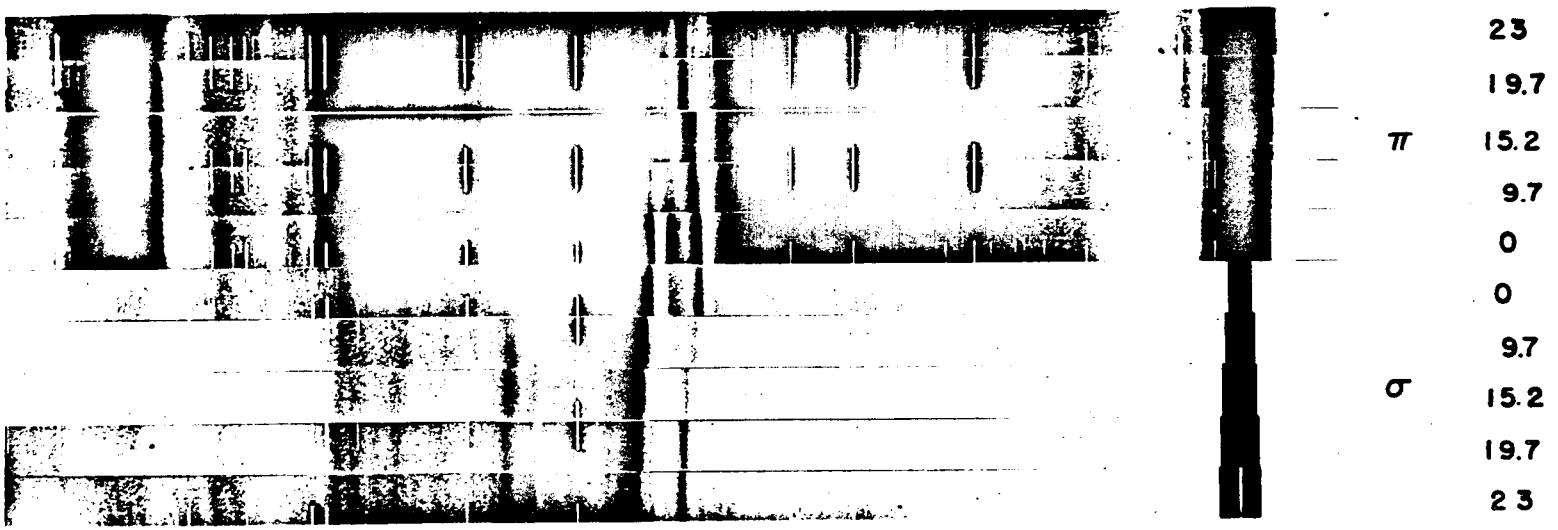

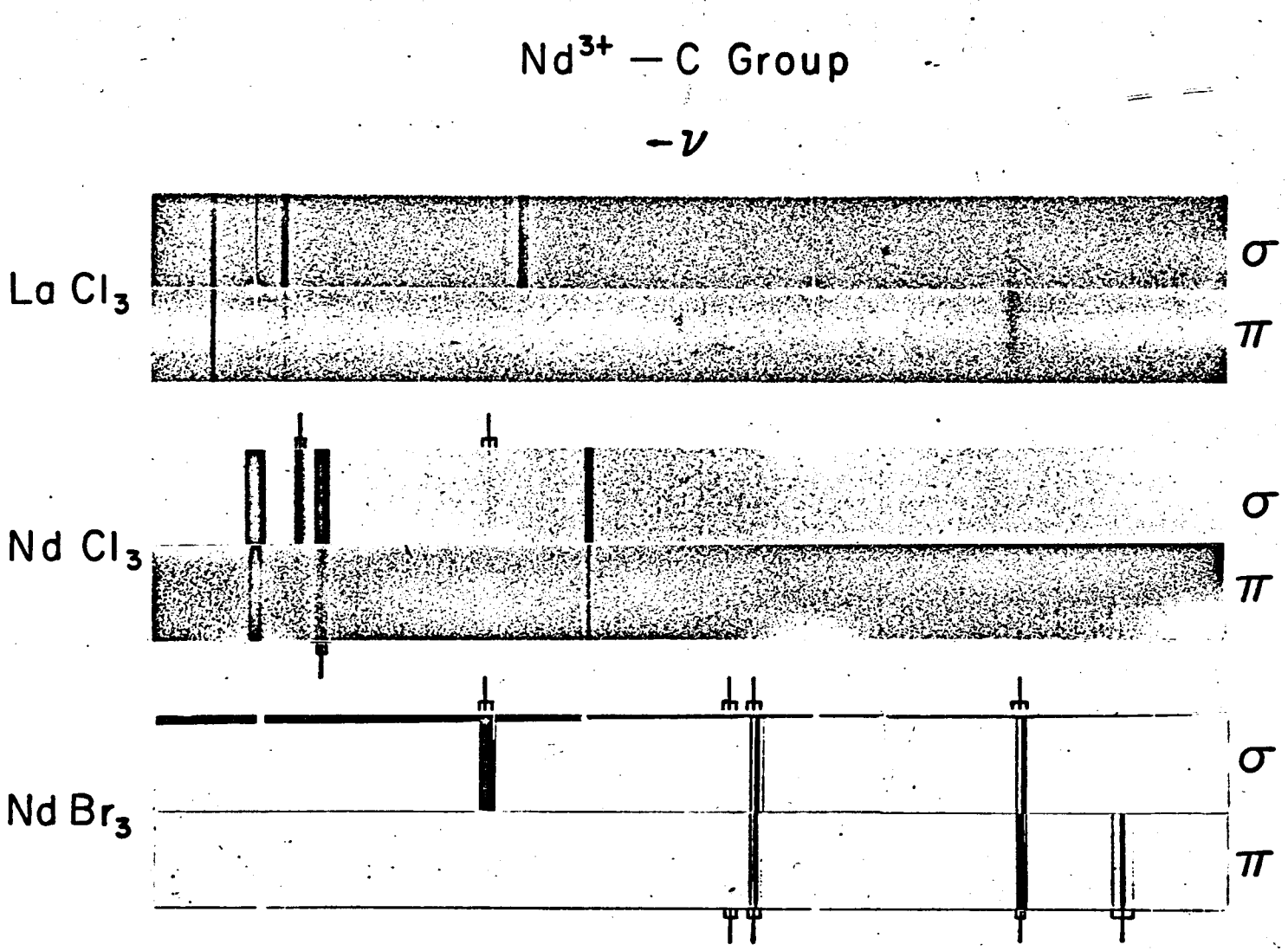

Figure 8

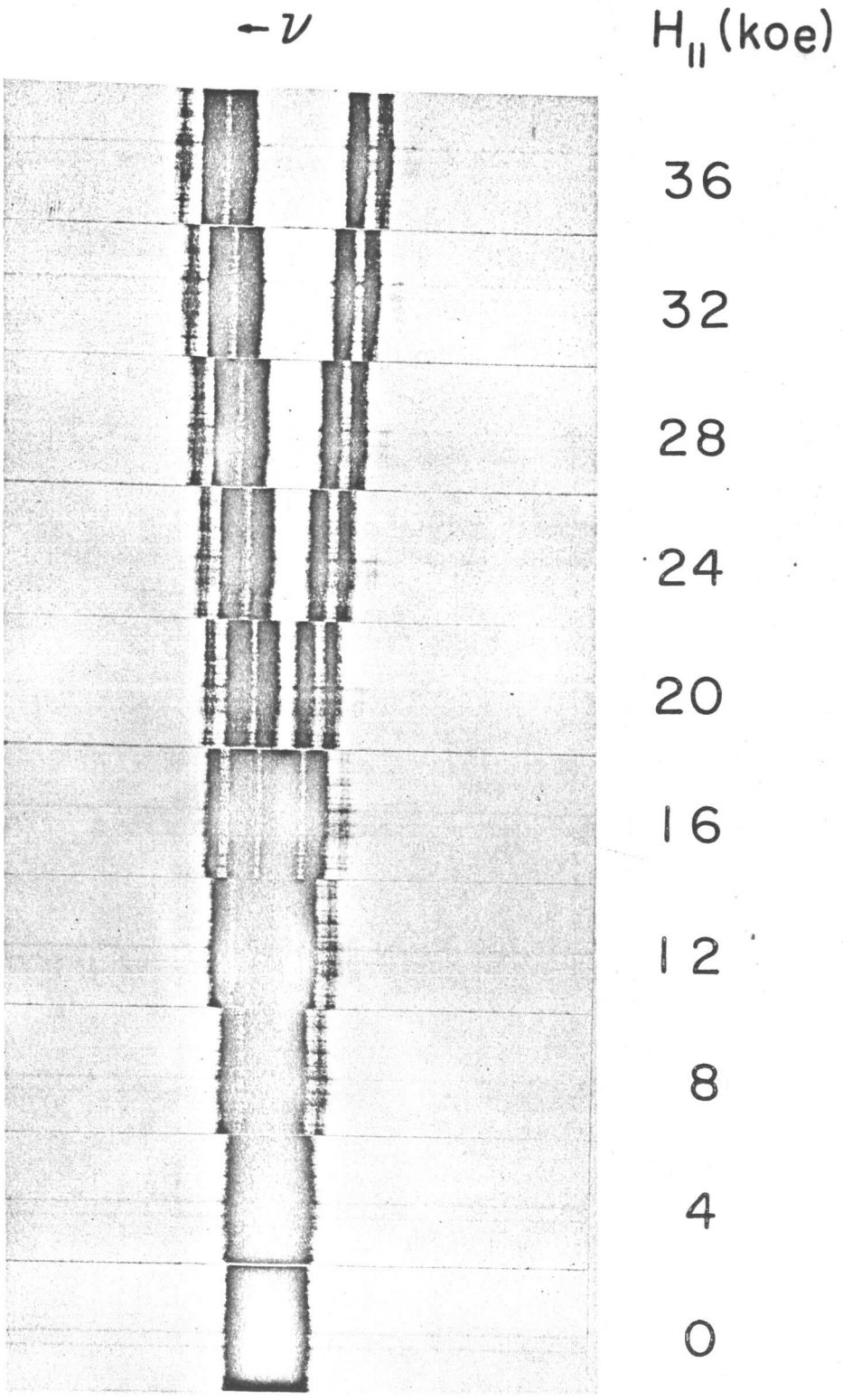

Figure 9. Parallel Zeeman splitting of I_1 (π) in $NdBr_3$. Bath temperature is 1.5° K. Region shown is centered at λ_{vac} = 4241 Å and is 5Å (30 cm^{-1}) wide.

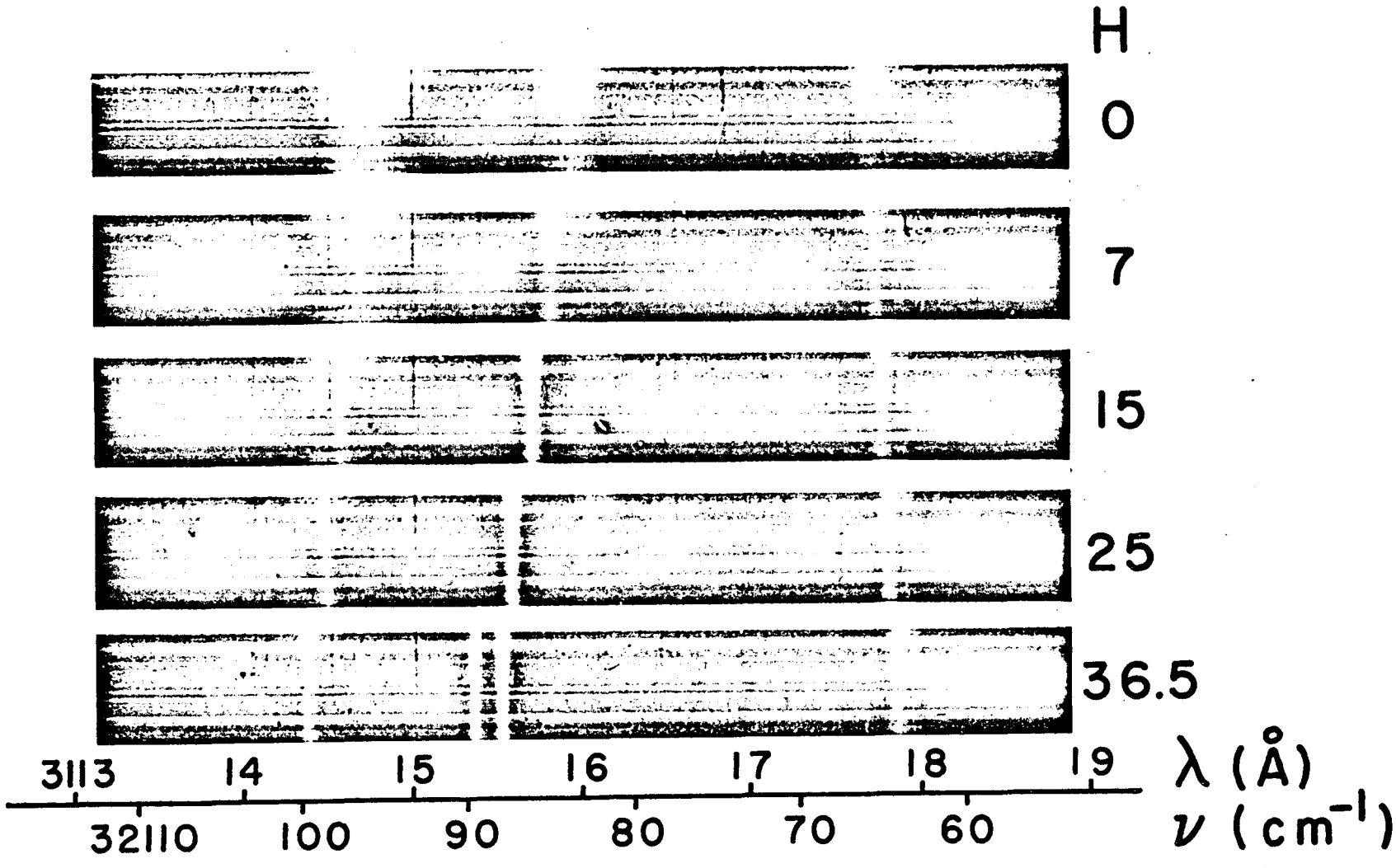
H
0
7
15
25
36.5
3113
14
15
16
17
18
19
λ (Å)
32110
100
90
80
70
60
ν (cm⁻¹)

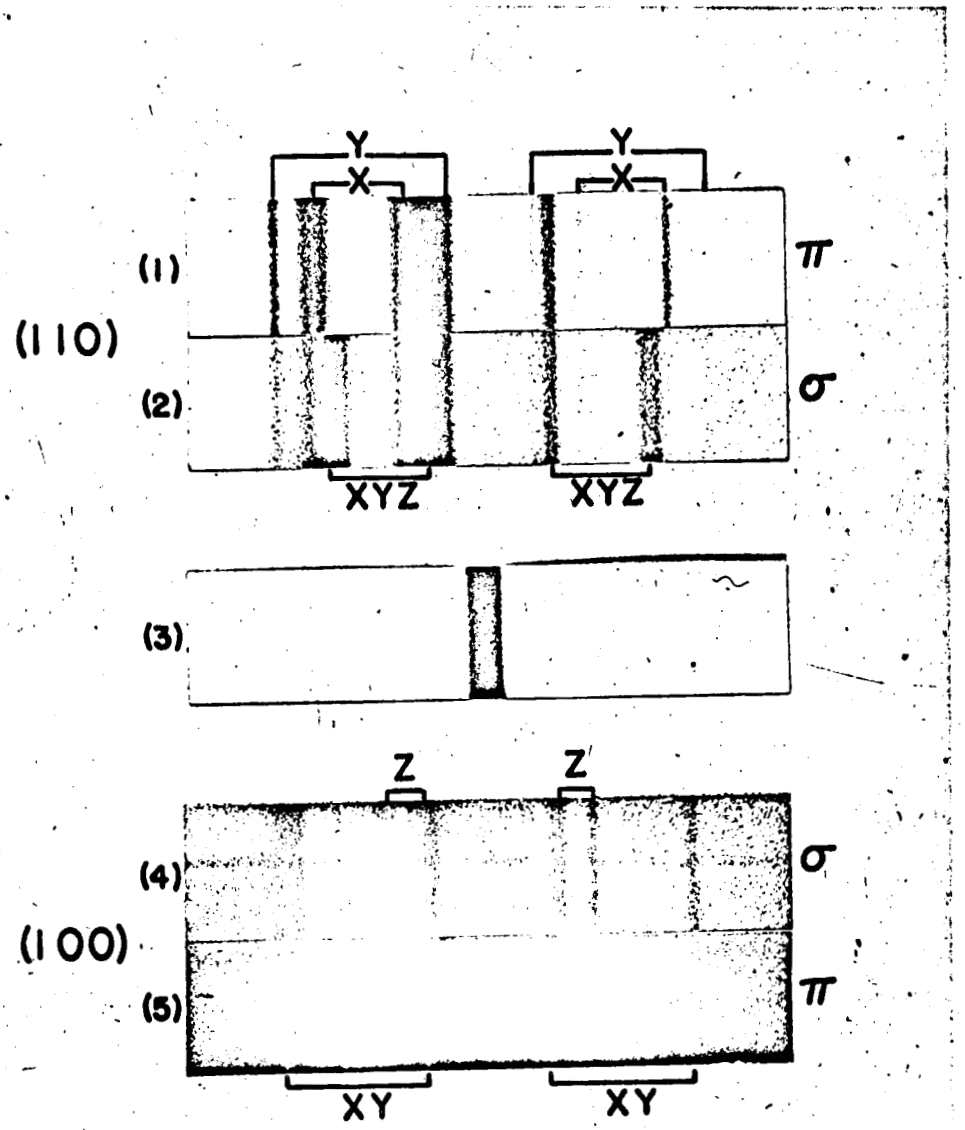

Yb^{3+} in YAG

Figure 11

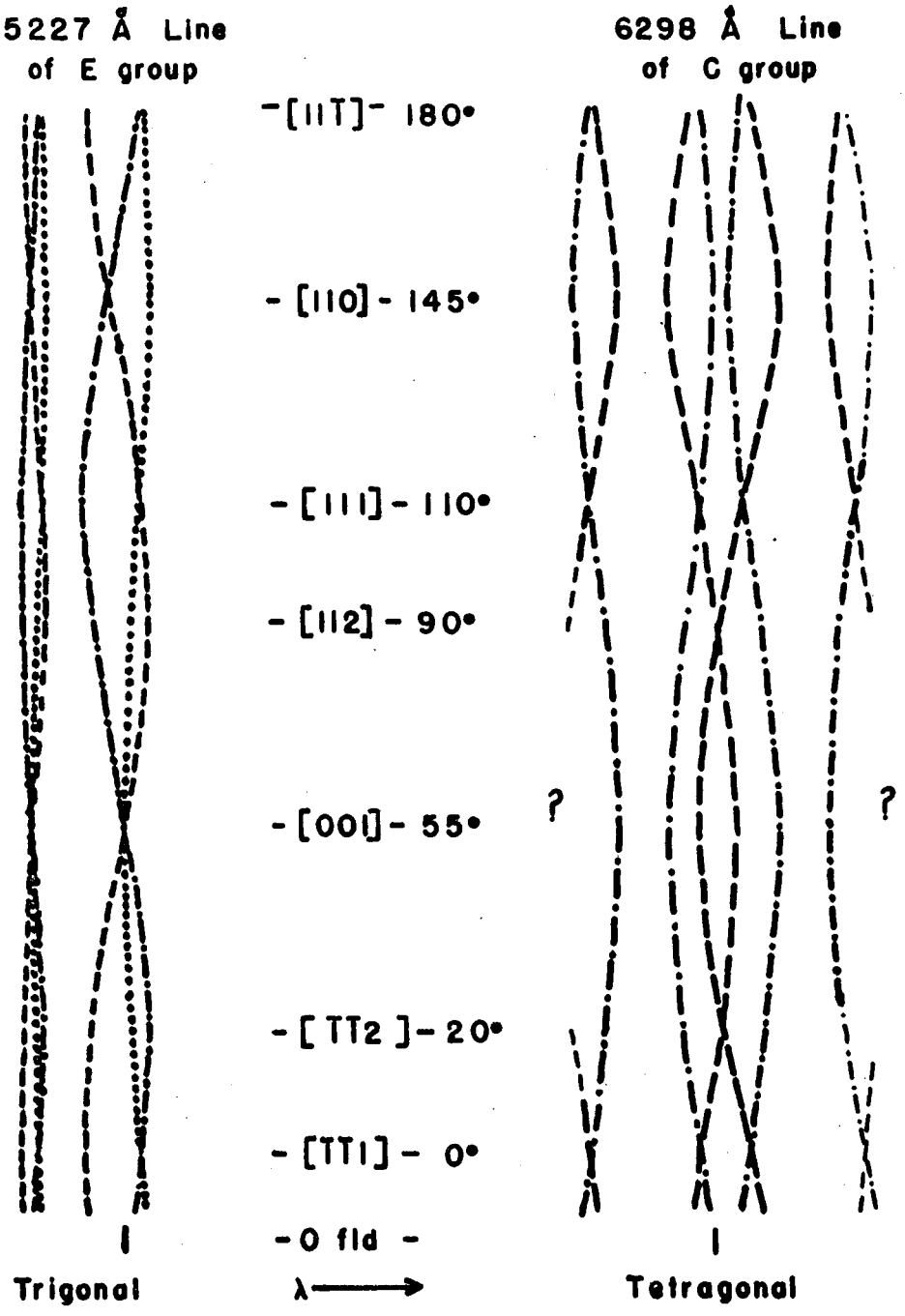

Figure 12. Composite showing the variation of Zeeman absorption spectra of type II $CaF_2:Nd^{3+}$ for rotation about the $[\bar{1}10]$ axis. The temperature is near 4.2° K and the field is 36,650 gauss.

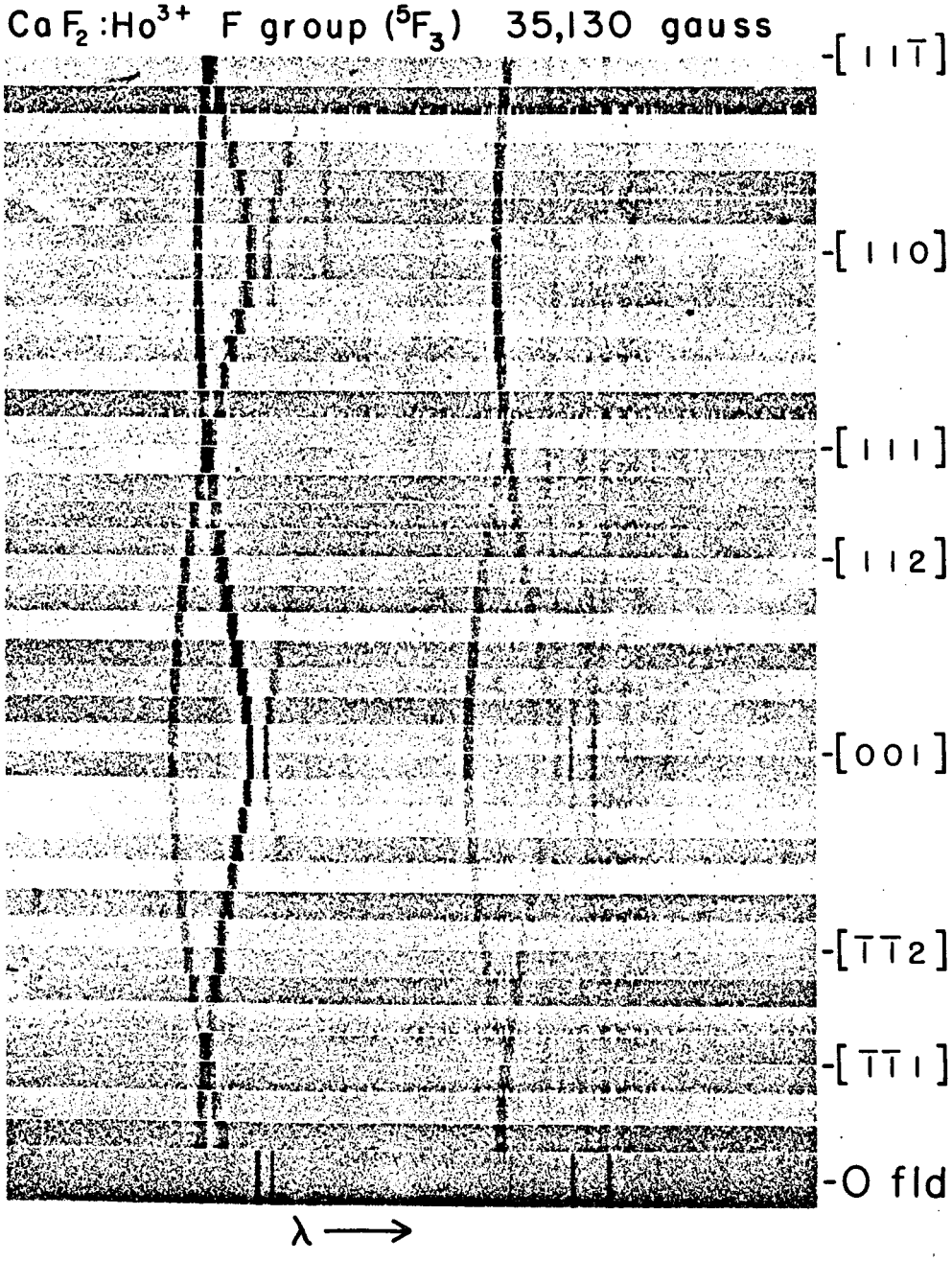
CaF2:Ho3+ F group (5F3) 35,130 gauss
-[11T̄]
-[110]
-[111]
-[112]
-[001]
-[T̄T̄2]
-[T̄T̄1]
-0 fld
λ ⟶

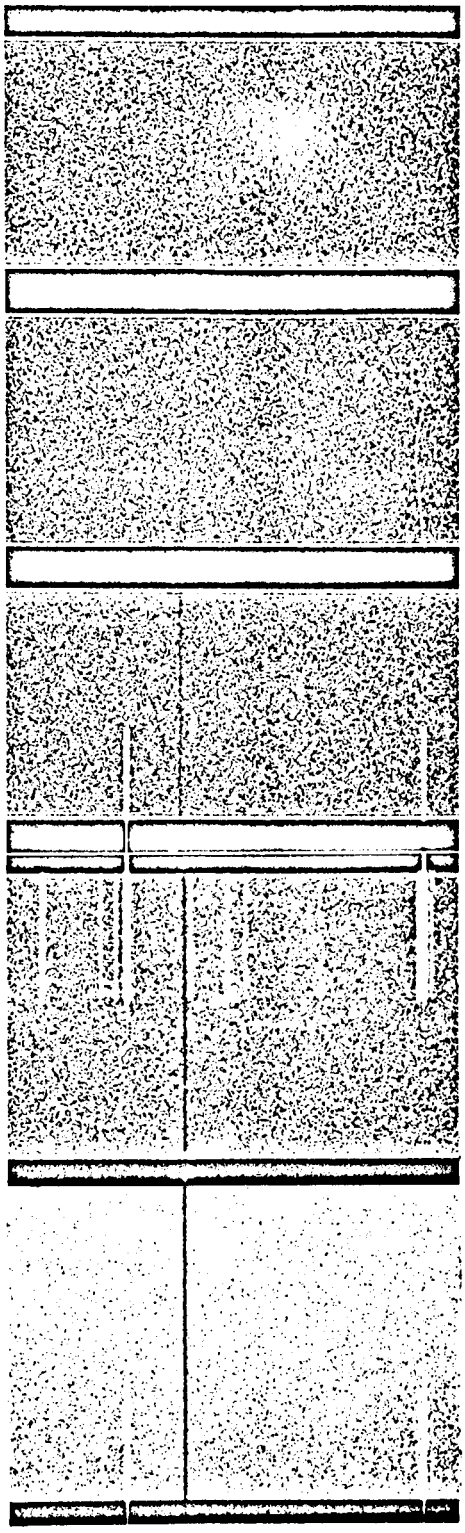

Fig 14 Composite

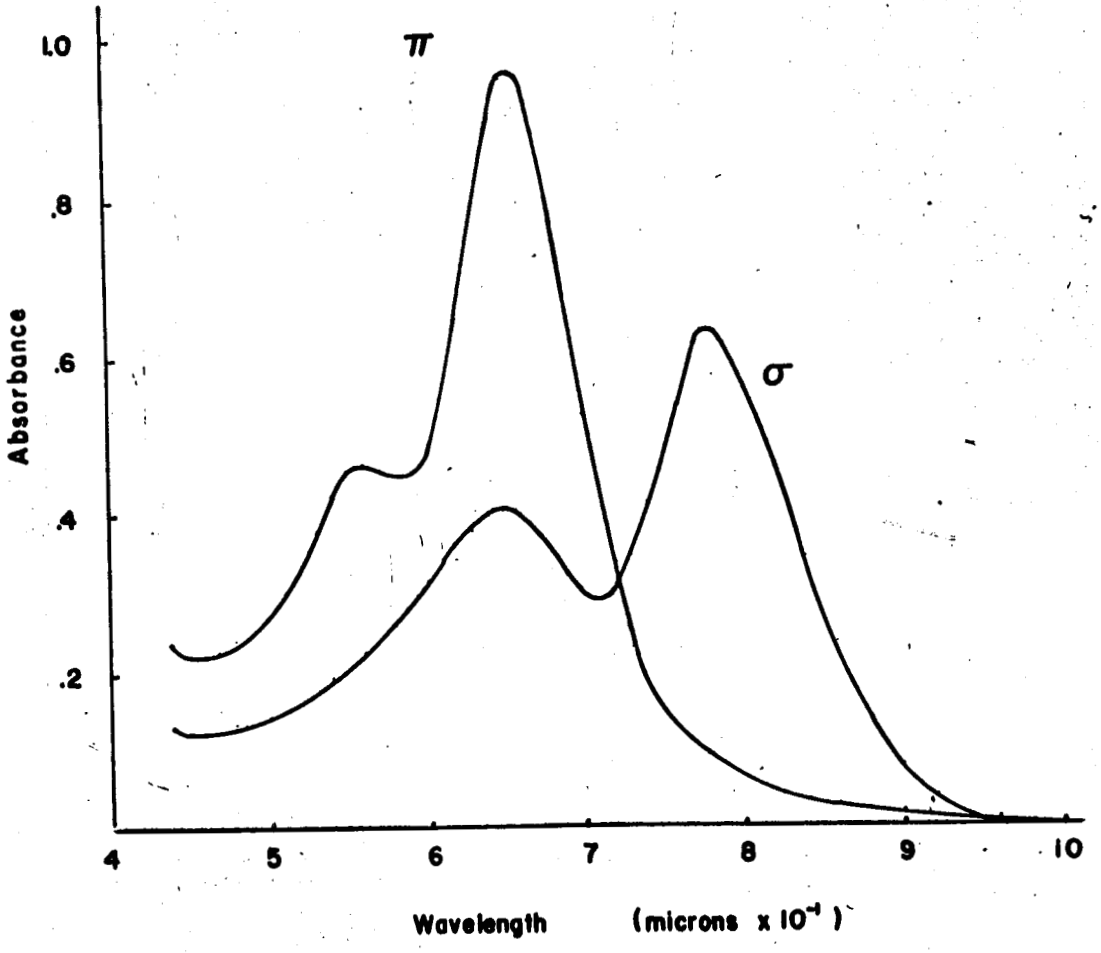

Figure N

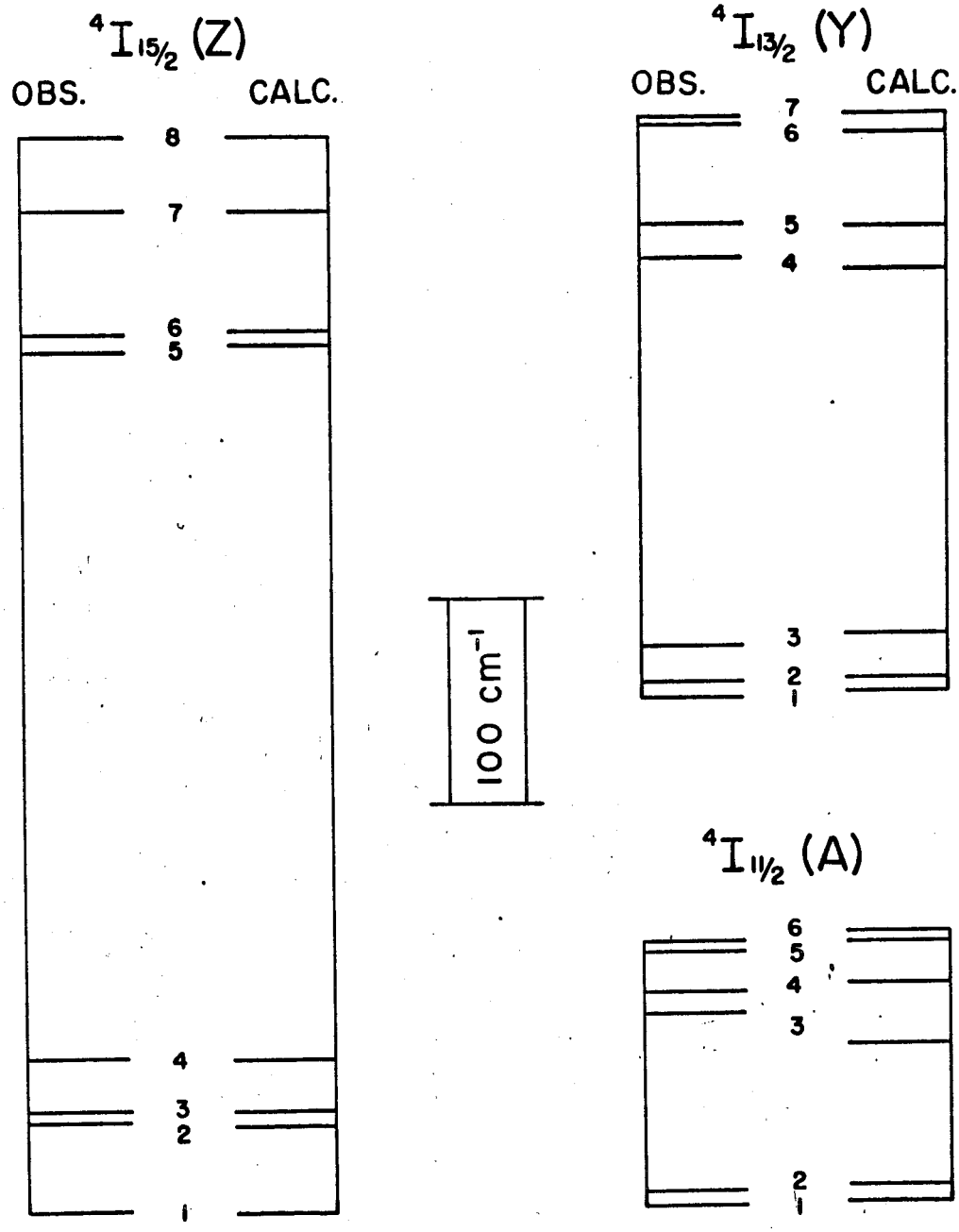

Er in Yttrium Gallium Garnet

Figure 16

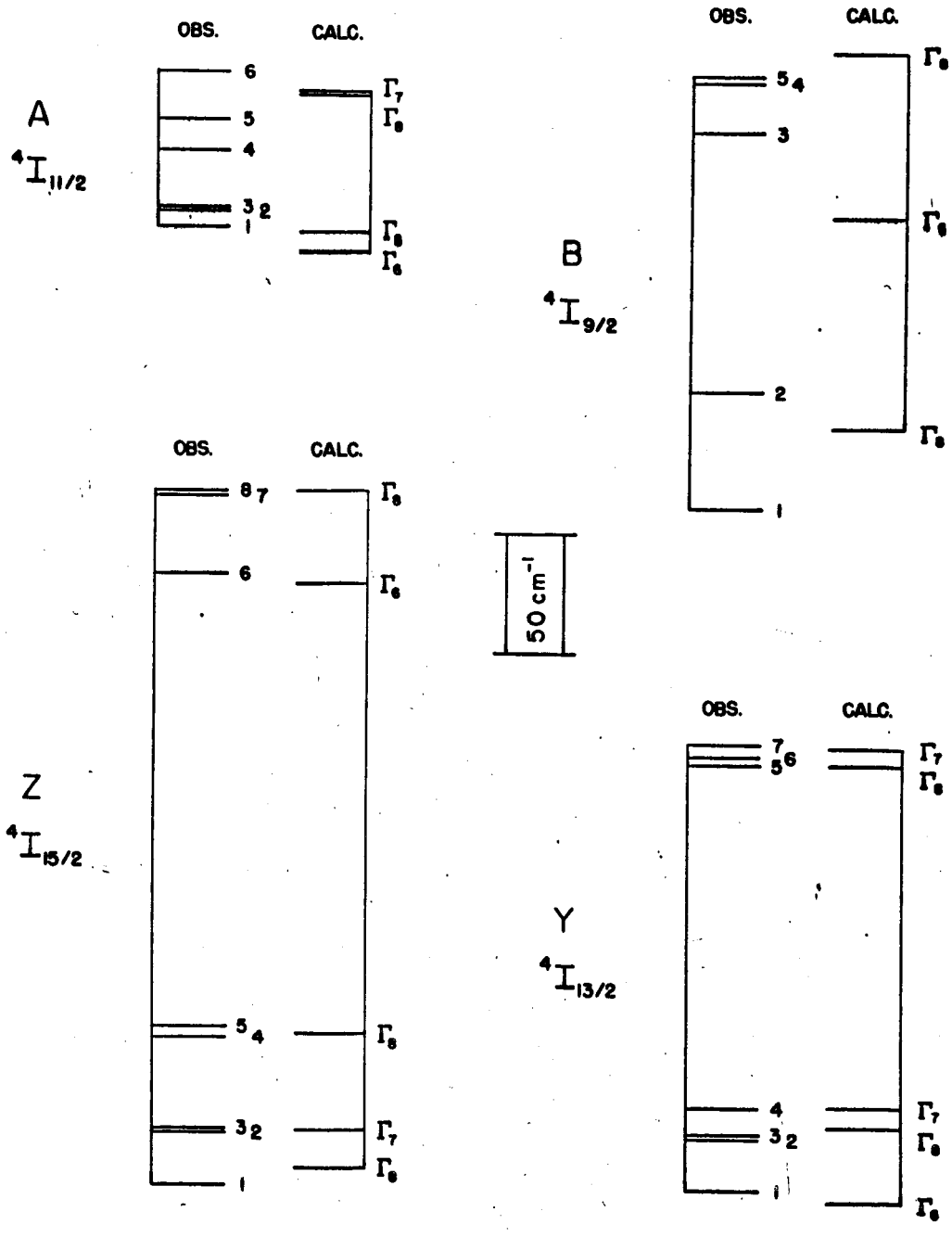
OBS.
CALC.
A
$^4I_{11/2}$
6
5
4
3 2
1
Γ_7
Γ_8
Γ_8
Γ_8
B
$^4I_{9/2}$
5 4
3
2
1
Γ_8
Γ_8
Γ_8
50 cm^{-1}
Z
$^4I_{15/2}$
8 7
6
5 4
3 2
1
Γ_8
Γ_8
Γ_8
Γ_7
Γ_8
Y
$^4I_{13/2}$
7 6
5
4
3 2
1
Γ_7
Γ_8
Γ_7
Γ_8
Γ_8

Figure 17

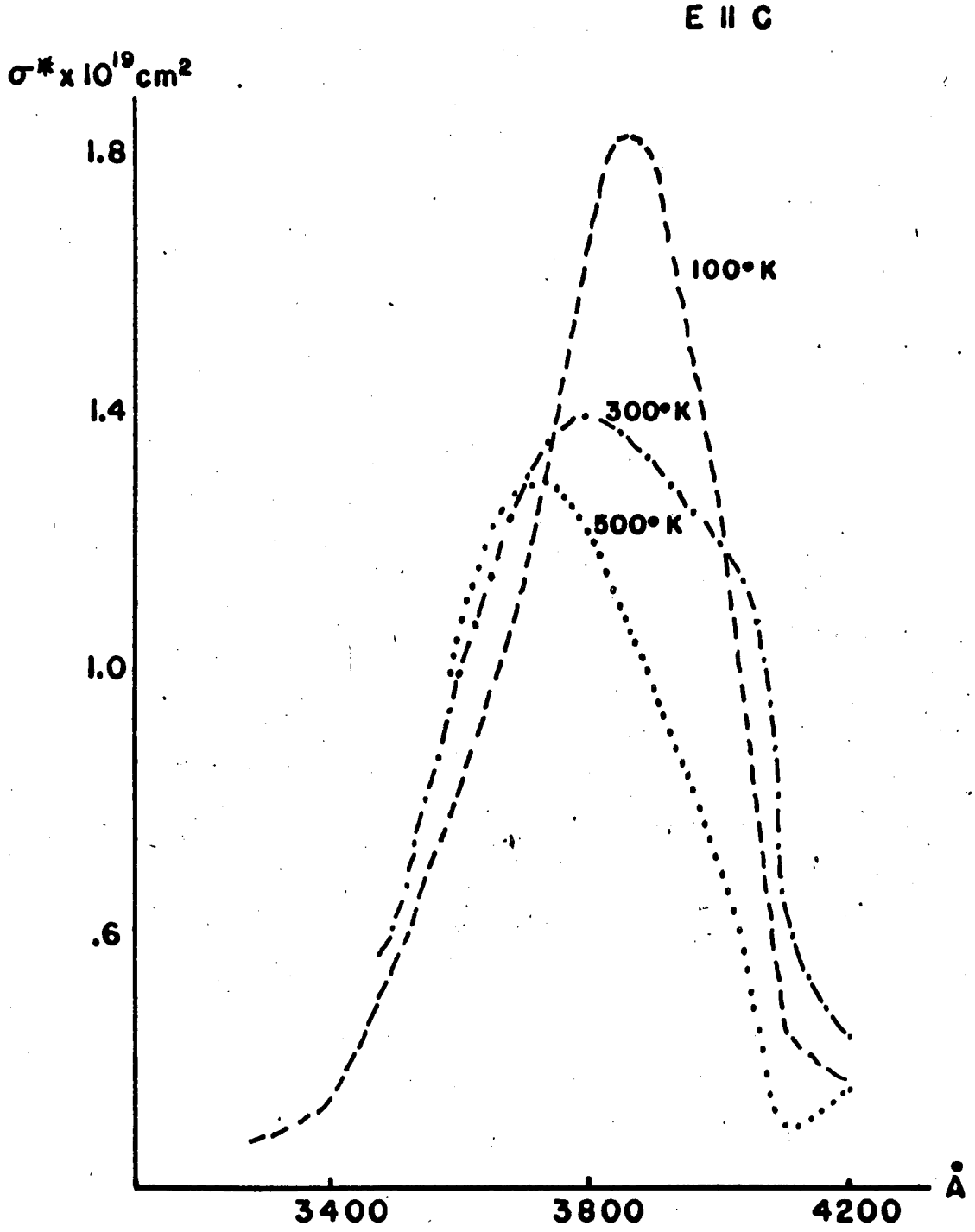

Figure 18